1969

The development of a water dynamometer for turbine test applications.

Mercer, Thomas Alexander

Monterey, California. U.S. Naval Postgraduate School

THE DEVELOPMENT OF A WATER DYNAMOMETER FOR TURBINE TEST APPLICATIONS

by

Thomas Alexander Mercer

United States
Naval Postgraduate School

THESIS

The Development of a Water Dynamometer
for Turbine Test Applications

by

Thomas Alexander Mercer

October 1969

The Development of a Water Dynamometer for Turbine Test Applications

by

Thomas Alexander Mercer
Lieutenant, United States Navy
B.S., United States Naval Academy, 1962

Submitted in partial fulfillment of the
requirements for the degree of

MASTER OF SCIENCE IN AERONAUTICAL ENGINEERING

from the
NAVAL POSTGRADUATE SCHOOL
October 1969

ABSTRACT

This study describes the design and development of a water dynamometer capable of absorbing and measuring a variable torque on a shaft rotating at velocities up to 20,000 revolutions per minute. The dynamometer was specifically designed to absorb a minimum of 117 horsepower at 10,000 RPM for use in the testing of small single stage turbines. The effects of various internal rotor and stator arrangements, water flow rates, internal clearances, and methods of torque variation and control were investigated. A method of extending the results of this study to the design of geometrically similar machines of larger size and increased torque absorption capacity was formulated.

TABLE OF CONTENTS

LIST OF TABLES

LIST OF ILLUSTRATIONS

TABLE OF SYMBOLS

Latin Symbol	Definition	Units
A	Water flow area or flat plate area	IN^2
a	Outer radius of flat plate	IN
b	Outer radius of center hole in a flat plate	IN
C_m	Moment coefficient	--
C_p	Constant pressure specific heat	$\frac{BTU}{lbm\text{-}^oF}$
D	Characteristic dimension-rotor diameter	IN
dm	Differential mass element	lbm
dV	Differential volume element	ft^3
$d\theta$	Wedge angle of a differential radial element	radians
E	Modulus of elasticity	lbf/IN^2
F_a	Axial force on front face	lbf
F_c	Centrifugal force on rotor	lbf
f	"is a function of"	--
g	Gravitational unit or gravitational constant	$32.174 \frac{ft\text{-}lbm}{lbf\text{-}sec^2}$
H	Head-energy per unit mass	$\frac{ft^2}{sec^2}$
Hg	Mercury	--
HP	Horsepower output of the turbine	hp
h	Rotor blade thickness	IN
I	Moment of inertia	IN^4
K_H	Head coefficient	--
K_P	Power coefficient -- machine constant	--
K_Q	Flow coefficient	--
K_T	Torque coefficient	--

K_μ	Viscosity coefficient	---
K_6	Specific Speed	---
k	Spring constant	$\frac{lbf}{IN}$
kHz	Kilohertz	$\frac{kilocycles}{sec}$
L	Length - used as a primary dimension	IN
M	Mass - used as a primary dimension	lbm
m	Inverse of Poisson's ratio	---
$\dot{m}$	Mass flow rate	$\frac{lbm}{sec}$
N	Revolutions per minute	RPM
N_{REF}	Referred RPM	RPM
N_s	Specific Speed	---
P	Power absorbed	hp
p	Pressure in the dynamometer	$\frac{lbf}{IN^2}$
psi	Pounds per square inch pressure	$\frac{lbf}{IN^2}$
$\frac{P_{to}}{P_2}$	Turbine pressure ratio	---
Q	Volumetric flow rate	$\frac{ft^3}{sec}$
R	Rotor radius	IN
R_i	Inner radius of an integrated interval	IN
R_N	Reynold's number	---
R_o	Outer radius of an integrated interval	IN
RPM	Revolutions per minute	RPM
T	Time-used as a primary dimension	sec
t	Thickness of a plate	IN
U	Rotor blade speed	$\frac{ft}{sec}$
V	Absolute velocity of flow leaving a rotor	$\frac{ft}{sec}$

W	Weight of a spring-mass system	lbf
w	Unit applied load on a plate	$\frac{lb}{IN^2}$
$\dot{w}$	Weight flow rate	$\frac{lbf}{sec}$
y_o	Static deflection of a spring-mass system	IN
z	Geopotential height	ft

Greek Symbols

α	"is proportional to"	---
β	Water flow divergence angle from rotor	deg
γ	Ratio of specific heats	---
Δh_{is}	Isentropic enthalpy drop across turbine	$\frac{BTU}{lbm}$
ΔT_{is}	Isentropic temperature drop across turbine	^oR
δ	Referred pressure	---
δ_T	Turbulent boundary layer thickness	IN
η_{ST}	Total to static efficiency	per cent
θ	Referred temperature	---
θ	Flow divergence angle from face grooves	deg
μ	Absolute viscosity of the fluid	$\frac{lbf\text{-}sec}{ft^2}$
ν	Kinematic viscosity of the fluid	$\frac{ft^2}{sec}$
ρ	Density of the fluid	$\frac{lbf\text{-}sec^2}{ft^4}$
Σ	Summation of terms symbol	---
σ_B	Bending Stress	$\frac{lbf}{IN^2}$
σ_c	Centrifugal stress	$\frac{lbf}{IN^2}$
σ_T	Total stress in the rotor	$\frac{lbf}{IN^2}$

τ	Torque absorbed	IN-lbf
ω	Angular velocity of the rotor	$\frac{\text{radians}}{\text{sec}}$
ω_n	Natural frequency-critical speed	$\frac{\text{radians}}{\text{sec}}$

I. INTRODUCTION

The Turbo-Propulsion Laboratory, Department of Aeronautics, of the Naval Postgraduate School has facilities for testing small axial and radial flow turbines at high pressure ratios, various axial and radial clearances, and at subsonic, transonic, and supersonic inlet velocities. The two primary facilities used for these investigations are the Transonic Turbine Test Rig, a single-stage axial turbine, and the Radial Turbine Test Rig, a dual discharge radial inflow turbine. Previous tests on these turbines have utilized an air dynamometer of commercial design to absorb and measure the power output of the turbine and to control the rotational velocity. However, this dynamometer, operating as an air pump, is incapable of absorbing sufficient power to properly limit the rotational velocity of the turbines to the range of interest for tests at transonic and supersonic rotor inlet velocities. The starting and off-design characteristics of the turbines could not be determined. Representative minimum operating speeds that resulted at elevated turbine pressure ratios with the air dynamometer set for maximum power absorption can be seen in Figure 28.

A dynamometer using water as the working medium was considered to offer the most practical means of absorbing increased torque. The feasibility of purchasing a water brake was investigated, but the dynamometers that were considered were not acceptable for several reasons. These included the operating characteristics of the machines, the cost involved, and the desire to have a water brake that was interchangeable with the air dynamometer on the existing test apparatus.

Historically, the principles involved in the design of hydraulic machines of the type envisioned have been known since proposed by Froude in 1877. Applications of the principles include fluid couplings used extensively by the automotive industries, windage loss considerations on partial admission turbines and astern turbines for marine applications, and the losses and flow characteristics associated with centrifugal pumps. Water brakes are used extensively in the testing of internal combustion engines where the installations are generally permanent and have larger rotor wheels running at maximum rotational velocities of about 4,000 RPM. A reference search revealed very little quantitative information or studies on the flow characteristics in these machines.

The theory of operation is based on the hydraulic resistance to the rotation of an impeller. This drag on the rotor results from form resistance, which is a function of blade shape and surface area normal to the plane of rotation, and surface friction which is influenced by the surface roughness and the flow parallel to the plane of rotation.

Reference 1 has categorized the existing machines into three basic types:

A) Disc Brake: A single disc or multiple flat rotor discs with small clearances between rotor casing. This type of brake is most often used for high speed applications. An analysis of disc friction effects is included in Section IV.

B) Pin Brake: The torque absorption is dependent on form resistance on pins or rotor blades on a meshed stator and rotor. This type of energy absorber is used for medium load applications and crude work where close torque control is not a consideration.

C) Fluid Brake: Energy is absorbed by the pumping action of an impeller fitted with vanes of a design that requires a considerable amount of torque to impart a circulation to the fluid and move it into a stator. This design is used for low to medium speeds and medium to high loads and relies on both form resistance and surface friction for power absorption.

A machine of type (C) can be visualized as being a very inefficient centrifugal pump where the rotor blades are designed to impart high rotational velocity to the fluid rather than a large pressure head. This high velocity is then decreased by a suitable stator arrangement that produces considerable turbulence in the flow. The useful energy is thus converted into internal energy (a temperature rise) rather than into static head as it is in the diffusor of a centrifugal pump.

A water dynamometer of the fluid brake type was selected as the only design capable of absorbing sufficient torque at the relatively high rotational velocities. A brake of suitable dimensions, and the associated hardware shown in Figures 1 through 6, was designed by Professor M. H. Vavra of the Department of Aeronautics. The present study is concerned with the installation and modifications to the brake that were undertaken to determine the optimum configuration and performance of the dynamometer and to investigate the flow phenomena that occur in machines of this type. All of the tests were conducted utilizing the Transonic Turbine Test Rig as the prime mover, as described by Commons [Ref. 2] and Lenzini [Ref. 3]. However, the dynamometer as developed could be used with the Radial Turbine or for other applications. The specific goal of this project was to develop a dynamometer capable of absorbing 738 in-lbs of torque at

10,000 RPM. This corresponds to 117 HP. These data correspond to the curves in Figures 26 and 27 which are labeled as minimum desirable.

The author gratefully acknowledges the guidance and inspiration provided by Professor Vavra. Thanks are also given to Mr. J. E. Hammer and his coworkers of the technical staff of the Turbo-Propulsion Laboratory for their many hours of assistance in modifying and operating the water brake and turbine test rig. The precise and expeditious work of Mr. M. O'Dea and his fellow machinists in the Postgraduate School Machine Facility is greatly appreciated.

II. DESCRIPTION OF APPARATUS

An overall view of the internal configuration of the water dynamometer appears in Figure 1. All the major components of the dynamometer are made of stainless steel (SS 301-303). A lever arm is rigidly attached to the back of the dynamometer assembly which is free to rotate, restrained only by a Wiancko force capsule that is used to measure the torque. This system will be described later in detail. The manner in which the brake is mounted to the dynamometer bearing stand can be seen in Figure 1 as well as in the photograph of Figure 2. The required adapters for changing from the air dynamometer to the water brake installation are shown in Figure 3.

Figures 4 and 5 show the complete installation. The overall dimensions of the brake are 10½" diameter by 2½" and the water chamber is 7"D x 1½". Water from a main enters the brake axially at the hub through a flexible reinforced plastic pipe at a flow rate between ten and thirteen gallons per minute. A flow honeycomb in the inlet pipe is used to insure that the inlet flow has no swirl component that could possibly affect the torque readout. An Iron-Constantan thermocouple was used to measure the inlet water temperature for experimental verification of the power absorbed. This thermocouple is not used in the normal turbine test configuration. The rotor assembly is rigidly attached to the turbine wheel being tested and turns at the same speed. As water enters the brake, the rotor imparts an angular velocity to the water and it is thrown radially outward in all directions by centrifugal force. The small clearance between the rotor nut (Part 2135-6, Figure 1) and inlet pipe and the relatively

large water flow rates insure that the water passages around the hub remain full. It was found that this is required for steady-state operation of the brake. The power produced by the turbine is absorbed by disc friction and form drag on the rotor turning in a ring of water. At the same time, the rotor accelerates the water ring and imparts kinetic energy to the flow. The water leaves the water chamber radially through holes in the shroud (Part 2134-1, Figure 1). An Iron-Constantan thermocouple measures the water exit temperature. Since the water enters axially with no angular momentum and is forced to exit radially with no angular momentum, the casing exerts a balancing torque on the water that is equal and opposite to the turbine torque. All of the rotational energy of the rotor is transmitted to the water and thence to the outer case. The force necessary to restrain the outer case from rotating is measured to determine the torque output of the turbine. The water passes radially from the shroud through two 0.75" diameter holes fitted with exit tubes. Two flexible pipes then lead to the water regulating valve assembly in Figure 6. Water from the two exit ports of the brake collects in the plenum, then passes the valve and valve seats to a single overboard drain. For all of the tests of this study, the water was not salvaged. However, for prolonged operation, the water could readily be put in the cooling water discharge lines of the compressor that provides the air supply for the tests. It would be cooled in the compressor's water tower and used to replenish the compressor cooling supply. A more involved closed water system with circulation through the water brake, a water cooler, and a pump could be utilized if required.

Increased throttling of the water brake and hence greater torque absorption is accomplished by partially closing the water regulating valve causing the water ring formed around the outer-periphery of the water chamber to move closer toward the axis. A greater length of the rotor blades is thus running in the water ring. A small electric motor is fitted over the end of the water regulating valve so that the extent of the water ring and torque absorption can be varied from the control room. For most test runs, the water regulating valve was closed to the maximum extent possible for a particular turbine pressure ratio under investigation. This resulted in maximum power absorption and the minimum speed obtainable for that particular pressure ratio. The water valve was then opened in increments to obtain the desired data at increased rotational velocities. An indication of the maximum power absorption point occurs when water starts to leak from the relief holes in the water brake adapters (Figure 3).

To prevent water from reaching the bearings and to increase torque absorption, the regulating valve was opened slightly from this point. When operating with a plexiglass front face on the dynamometer, the point of maximum energy dissipation can be determined with operating experience by the appearance of the water ring.

It was found that the introduction of air pressure at the hub of the back face (2133-1, Figure 1) was useful for several reasons. It helped to prevent water leakage from the adapter holes. It also resulted in more steady operation of the water brake by equalizing the axial force between the front and back faces of the rotor, prevented local cavitation, and stabilized the extent of the water ring by retarding foaming. An air supply was connected to three taps located

at the minimum practical radius of the back face (Figure 2). Approximately 25 psi air pressure was set before the run and proved to be advantageous for all operating conditions.

The Transonic Turbine Test Rig, hereafter referred to as the TTR, is described extensively by Commons [Ref. 2] and Lenzini [Ref. 3]. Only the features of the TTR of direct application to this study will be further described. The turbine rotor that is being tested is attached to a shaft supported in a bearing housing by two matched sets of high precision ball bearings. A steel quill shaft connects the rotor shaft to the water brake shaft running through the Vortec Air Dynamometer bearing stand. Both sets of bearings are lubricated by oil mist. The water brake adapters (Figure 3) permit ready interchangeability when shifting from low speed-high power absorption requirements where the water brake is used, to high speed applications with lower power absorption requirements utilizing the air dynamometer. The changeover has been accomplished in less than thirty-five minutes between rotor shutdown and restart including rechecking the calibration of the dynamometer force capsule.

A six-lobe flux cutter on the shaft used in conjunction with a magnetic pickup provides the means of determining turbine and water brake rotor speed. The revolutions per minute are read directly on a Hewlett-Packard electronic counter in the control room.

A twenty-inch lever arm is rigidly attached to the dynamometer housing (Figure 2). The free end of the arm has a ball fitting that rests in an oversized slot cut in an aluminum block (Figure 8). The block is attached to the bottom of a Wiancko Engineering Company Model F1009 force capsule. The capsule uses a phase-shift frequency-modulated oscillator to sense an air gap change caused by the

proportional deflection of a thin ring under load. The force capsule is attached at the top to a Fafnir Self-Aligning Rod End mounted in a support bracket. The linear range of the oscillator is from ten to twelve kHz with a range of 0 to 50 pounds of force. The torque exerted on the dynamometer housing is transmitted to the arm and produces a tension load that is taken up by the force capsule. The force gage limits the angular rotation of the dynamometer housing to about a half degree. A plexiglass case around the force capsule helps to minimize temperature effects and protects the capsule.

An eye is attached to the bottom of the aluminum block for calibrating the force pickup with known weights (Figure 9). Calibration is performed with the dynamometer arm in position, and this is taken as the zero load condition. A no-load reading of 10 kHz is set on a Monsanto Model 100A digital readout. Forty pounds of weight are then applied (corresponding to 800 in-lbs. of torque with the 20-inch moment arm), and the bandwidth is adjusted to 12 kHz. The zero no-load reading is again checked. Linearity is checked with one-half of the full load, and an 11 kHz reading should result. If the output is not 11 kHz, the reading is changed in the direction of the error by an amount equal to three times the error. The full and no-load readings are then readjusted to 10 and 12 kHz. The procedure is repeated until linearity is achieved. System hysteresis and repeatability is checked by loading the force capsule in five-pound increments from zero to full load and then decreasing the load in like increments. A typical calibration curve is shown in Figure 10.

After the dynamometer has been calibrated, the lever arm is lifted off the aluminum block by hand to record a no-load tare reading of the

force capsule. This provides a means of checking the capsule during the run for variation with temperature. The dynamometer arm is lifted periodically during the run, and the reading is compared with the original tare reading. The dynamometer output is then corrected by the difference of the two readings. This correction procedure is particularly important when using the air dynamometer because the hot exhaust air from the dynamometer discharges into the region where the force capsule is mounted. Although the force capsule is supposed to be temperature insensitive in the test range, it was previously found that heating or cooling caused large variations in the output signal [Ref. 2]. The force capsule and support structure is enclosed in a wooden box (Figure 9), and air at constant temperature is blown through the enclosure by a fan. When using the water brake, temperature variations on the force capsule are caused primarily by changes in the test cell temperature. The temperature drop in the turbine is proportional to the work generated by the turbine stage, and variations in turbine exhaust air temperature during a run can cause the test cell temperature to vary.

The water for the dynamometer is supplied by a water tap located in the test cell. Maximum water flow rate is approximately thirteen gallons per minute. For ease of manipulation and control upon starting the turbine, and also to help prevent water supply surges from affecting the water supply to the brake, two water flow valves were located near the water brake. These valves are manipulated to obtain the entire range of water flow through the brake from no flow (brake bypassed) to the maximum available. After several runs of the dynamometer, it was found that a more steady operation resulted with maximum water

flow through the brake, and flow manipulation with the water valves was used solely for start-up and shutdown.

The water flow rate can be measured by collecting and weighing the water leaving the brake in a large barrel and calculating the gallons of flow per minute from the change in weight per time interval. With the water temperatures recorded at brake inlet and exit, the power absorption was calculated for verification with the force capsule output. For this method of torque absorption measurement to be practical for turbine tests, a calibrated water flow nozzle would have to be installed in the water exit pipe.

During the development process, pressure taps were located at points of interest on the front and back face of the water brake to sample the water chamber pressure at various radii. These taps were connected to direct reading Bourdon gages with a pressure range between 30 inches of mercury vacuum and 250 pounds per square inch gage. These pressure taps are not used during normal water brake operation.

An accelerometer mounted on the dynamometer bearing stand provides a means of monitoring the vibration pattern of the water brake. The output signal of the accelerometer is displayed on a Singer Panoramic Analyzer and on an RMS millivoltmeter in the control room. The RMS readouts were used primarily as a relative indication of the vibration level for various stator arrangements and for comparison with known acceptable values observed when using the air dynamometer. They were used to give an indication of the onset of cavitation and water ring breakdown upon dethrottling the water brake from maximum torque absorption. However, after gaining operating experience with the water

brake, these conditions could be anticipated by observing the appearance of the water ring through the plexiglass face and by fluctuations in the rotor RPM. For early runs, a Consolidated Electrodynamics Corp. hand-held vibration meter was used directly on the water brake to determine the vibration level as the operating conditions were changed.

All of the significant turbine pressures were measured on a mercury manometer board except the pressure differential across the air flow nozzle which was read on a water filled U-tube. The data were reduced on an IBM 360/67 computer using the TTR program developed by Esdaile [Ref. 4].

The original design components (Figs. 14 and 15) can be utilized for five different rotor configurations. Any rotor-spacer arrangement that is 0.75 inch or less between the rotor hub and rotor nut (2135-4 and 2135-5, Figure 1) is acceptable, but in order to maximize the form drag torque absorption, two teethed rotors (Figure 14) were mounted back to back for Rotor Configuration 1 (Figures 1, 11 and 12) and tested on Runs 1 to 19. Two rotors similar to Figure 14 of 6.50" diameter and .220" thickness were manufactured and tested on Runs 20 to 28. The stress calculations for these rotors are given in Appendix 1. Runs 20 to 23 utilized Rotor Configuration 2 (Figure 11) while Rotor Configuration 3 was used on Runs 24 and 25. The 6.50" rotors were placed together in a configuration similar to Rotor Configuration 1 of increased diameter for Runs 26 to 28.

III. THE DEVELOPMENT PROCESS

The original test of the water dynamometer was conducted in February 1967. Rotor Configuration 1 (Figure 11) was assembled and dynamically balanced, and the water brake was mounted as shown in Figure 1. A thermocouple was installed in the collecting plenum of the water regulating valve (Figure 6) to monitor the water temperature leaving the brake. A run without water was made to 12,300 RPM and an acceptable maximum vibration of approximately 1 g was observed. The water brake was run for ten minutes at this speed and no mechanical difficulties were noted.

The turbine was shut down and the water inlet valve was placed in the full open position with the water regulating valve open. This resulted in leakage from the holes in the water brake adaptors (Figure 3) and the water was shut off. It was decided to have the rotor turning slowly before opening the water inlet valve so that the centrifugal force would prevent water from flowing to the vicinity of the hub. The rotor was set at 800 RPM and water was again introduced to the dynamometer. This resulted in a very smooth start and no leakage. The water ring seemed to form immediately, and vibration indications were normal. Turbine drive air was gradually increased during the start to offset the drag on the rotor and to maintain 1000 RPM. The water inlet valve was opened all the way. This starting procedure has been used for all subsequent tests.

The angular velocity was increased in steps to 10,000 RPM and vibration indications remained normal. However, the dynamometer output remained constant at approximately 24 counts throughout the speed increase.

With the rotor turning at 10,000 revolutions per minute and with a water flow rate of 13 gallons/minute, the water regulating valve was gradually closed to increase the torque absorption by forcing the water ring to move in radially around the rotor.

Shortly after a slight reduction in the water flow rate was noticed, moderate vibration and surging occurred in the brake. Vibrations were heaviest in the axial direction. The water exit temperature increased about $4^{o}F.$, but no increase occurred in the dynamometer torque output. Operating conditions returned to normal upon opening the water regulating valve slightly. The RPM was then set to 11,000 to determine whether the torque absorption increased with an increase in angular velocity. No torque increase was noted. Shortly thereafter, smoke and sparks were observed in the vicinity of the dynamometer shaft spline and an emergency shutdown was accomplished in approximately ten seconds. Upon disassembly, it was found that the dynamometer bearings had seized. No damage occurred in the water brake assembly.

The development phase of the water dynamometer which is the primary subject of this study was started in January 1969. In an attempt to explain the problems encountered on the original run, the critical speed of the rotor shaft was rechecked and found to be 65,800 RPM (Appendix B). This is well above the operating range of the turbine-water brake combination having a maximum allowable angular velocity of 20,000 RPM due to stress considerations. The other primary cause of trouble was considered to be the onset of cavitation on the back face of the rotor. This was a distinct possibility because inlet water under pressure enters only at the front of the

rotor while the water is pumped equally from the front and back sections of the water chamber by the rotor. If the vapor pressure of the water were reached in the back chamber, local boiling would occur, and unsteady operation and possibly rotor damage could result. The reduced pressure would tend to pull water through the rotor teeth into the rear area, thereby increasing the pressure. A high-frequency cycling with large variations in axial force on the rotor could occur. Two possible solutions to this problem were to introduce air or water under pressure through the back face (2133-1, Figure 1) of the dynamometer or to install a small check valve on the back face that would open to admit atmospheric air when a vacuum developed in the chamber. It was decided to install pressure taps at five different radii on the back face and eight locations on the front face of the dynamometer to sample the pressures that resulted. An air supply was available in the test cell to pressurize the taps as necessary to prevent cavitation.

Another possible source of trouble on the original run was that water entering the brake through the small annular passage around the rotor nut (Figure 1) could exert an excessive axial force on the rotor. However, it was felt that the bearing problems would have appeared earlier when the water flow was maximum if this was a primary area of concern. Therefore, enlarging of the flow passage or installation of water baffles was held in abeyance pending further developments.

The oil mist system to the bearings was checked to insure adequate lubrication. The installation of thrust bearings was not considered feasible due to the major modification of the bearing assembly that would be required. The balls of a thrust bearing would have to be sufficiently constrained to prevent them from moving outward under the large centrifugal forces. Also, the installed high-shouldered precision bearings have considerable thrust capacity.

A summary of the steps in the development phase appears in Table II and is shown graphically in Figures 26 and 27. For Run 1, the water brake configuration of Figure 1 was utilized with the addition of pressure taps at different radii with increments of 0.25" on the front and back faces. A dry run was made to 12,000 RPM and vibration readings well below 1 g resulted.

The angular velocity was then decreased to 1000 RPM and water was introduced to the brake. No appreciable torque absorption or pressure increase at the taps resulted. The RPM was increased to 4,000 in an attempt to form the water ring, but it appeared that a water-air mixture was being thrown around the case in a random manner by the rotor. Surges in the water supply and extreme sensitivity to water throttling prevented the recording of significant data. Attempts to regulate the water flow caused leakage from the adapter holes.

It is significant that neither in this run nor in any subsequent run have the large axial vibrations and the bearing problems of the original run been observed. It is surmised that either when the brake was filled with water with zero angular velocity or when the water regulating valve was closed in an attempt to obtain torque absorption on the original run, water flowed into the bearings through the labyrinth between the rotor shaft and casing-adaptors (Figure 1) and precipitated failure. During the development phase, water has been driven from the adaptor holes on several occasions by forcing the water ring in around the hub. However, it appears that when the rotor is turning and the oil mist to the bearings is turned on, very little water reaches the bearings through the labyrinth.

rotor while the water is pumped equally from the front and back sections of the water chamber by the rotor. If the vapor pressure of the water were reached in the back chamber, local boiling would occur, and unsteady operation and possibly rotor damage could result. The reduced pressure would tend to pull water through the rotor teeth into the rear area, thereby increasing the pressure. A high-frequency cycling with large variations in axial force on the rotor could occur. Two possible solutions to this problem were to introduce air or water under pressure through the back face (2133-1, Figure 1) of the dynamometer or to install a small check valve on the back face that would open to admit atmospheric air when a vacuum developed in the chamber. It was decided to install pressure taps at five different radii on the back face and eight locations on the front face of the dynamometer to sample the pressures that resulted. An air supply was available in the test cell to pressurize the taps as necessary to prevent cavitation.

Another possible source of trouble on the original run was that water entering the brake through the small annular passage around the rotor nut (Figure 1) could exert an excessive axial force on the rotor. However, it was felt that the bearing problems would have appeared earlier when the water flow was maximum if this was a primary area of concern. Therefore, enlarging of the flow passage or installation of water baffles was held in abeyance pending further developments.

The oil mist system to the bearings was checked to insure adequate lubrication. The installation of thrust bearings was not considered feasible due to the major modification of the bearing assembly that would be required. The balls of a thrust bearing would have to be sufficiently constrained to prevent them from moving outward under the large centrifugal forces. Also, the installed high-shouldered precision bearings have considerable thrust capacity.

A summary of the steps in the development phase appears in Table II and is shown graphically in Figures 26 and 27. For Run 1, the water brake configuration of Figure 1 was utilized with the addition of pressure taps at different radii with increments of 0.25" on the front and back faces. A dry run was made to 12,000 RPM and vibration readings well below 1 g resulted.

The angular velocity was then decreased to 1000 RPM and water was introduced to the brake. No appreciable torque absorption or pressure increase at the taps resulted. The RPM was increased to 4,000 in an attempt to form the water ring, but it appeared that a water-air mixture was being thrown around the case in a random manner by the rotor. Surges in the water supply and extreme sensitivity to water throttling prevented the recording of significant data. Attempts to regulate the water flow caused leakage from the adapter holes.

It is significant that neither in this run nor in any subsequent run have the large axial vibrations and the bearing problems of the original run been observed. It is surmised that either when the brake was filled with water with zero angular velocity or when the water regulating valve was closed in an attempt to obtain torque absorption on the original run, water flowed into the bearings through the labyrinth between the rotor shaft and casing-adaptors (Figure 1) and precipitated failure. During the development phase, water has been driven from the adaptor holes on several occasions by forcing the water ring in around the hub. However, it appears that when the rotor is turning and the oil mist to the bearings is turned on, very little water reaches the bearings through the labyrinth.

For Runs 2 through 6, water was supplied to the brake from a barrel of water by an electric pump. Water from the water regulating valve flowed back into the barrel. Since very little torque was being absorbed, no appreciable increase in the water temperature resulted in the passage through the brake. This arrangement resulted in a more steady water supply than from the test cell tap. The water was colored to facilitate flow visualization.

For Run 2 a drain hole was drilled at 1.75" radius in the front face (2133-2, Figure 1) in an attempt to control the extent of the water ring by preventing water from approaching the hub. At 4,000 RPM, the water regulating valve was slowly closed with no appreciable increase in torque. The exit valve was then closed completely, and the dynamometer was filled until water flowed from the drain. The inlet valve was closed and torque, pressures and water temperature in the brake were monitored. No increase was noted in these parameters.

A clear plexiglass face with an aluminum retaining ring to distribute the bolt stresses was machined for use on Run 3 and all subsequent runs. This enabled the operator to visually control the extent of the water ring and observe the flow characteristics in the dynamometer.

A strobotac was used to verify the rotor RPM and to determine the rotational velocity of the water ring.

During Run 3 it was determined that the water ring was forming in a parabolic shape due to the centrifugal force exerted by the rotor. With a small amount of water throttling, only the tips of the rotor blades were running in the water ring, but the ring extended almost to the hub on the front and back faces. Attempts to increase the torque absorption by increased water regulation resulted in water

pouring from the adaptor holes. The water ring was observed to be turning at approximately one half the rotational velocity of the rotor as predicted by Schlichting [Ref. 5].

It was determined that sufficient torque absorption could not be achieved solely through the disc friction effects caused by the shearing of the fluid between the rotor and the stationary casing (Section IV). Rotational stresses and space considerations limit the maximum disc radius, and mechanical considerations dictate a minimum clearance between rotor and casing.

For the large energy absorption required, the water ring must be formed and accelerated by the rotor to increase its kinetic energy. The fluid must then impinge on a stator where the kinetic energy is converted into internal energy (temperature rise) through turbulent deceleration (Section IV). The rotational energy of the rotor is thus transferred to the case where it is measured.

During the development phase, nine different stator configurations were tested to determine the optimum internal design of the dynamometer. Each of the stators used was symmetrical with respect to the mid-plane of the rotor with a similar stator arrangement mounted on the inside of both the front and back faces. Only the front face half of the stator configurations is shown in the drawings (Figures 16-25) unless indicated otherwise. Radial water exit slots leading to the outer shroud (2134-1, Figure 1) were located over the entire width of the rotor blade tips.

The stator half that was attached to the front face for Stator Configuration 1 is shown in Figures 16 and 17. The wedges at the outer periphery extend over the tips of the rotor blades. The raised portions

on the smaller radius section were designed for axial clearances of 0.020" from the rotor blade. The follow-on stator configurations (Figures 18 to 26) are shown only in face-on views for clarity. They are also characterized by an outer periphery that extends over the rotor tips and by a slotted inner radius section with small axial clearance. All the stators were machined from clear plexiglass for ease of manufacture and modification, and to facilitate flow visualization. It was first feared that the low impact strength of plexiglass might cause the stators to erode rapidly from cavitation and turbulent flow; however, the plexiglass held up very well with use. It is felt that this good performance occurred because acrylic plastic is very resilient and was able to yield and return to its original shape under localized loading conditions. The final optimum stator arrangement was manufactured from stainless steel for permanent use. The development phase was characterized by changing a single parameter for each additional run and determining the effect of this change. Before each stator configuration was manufactured an attempt was made to determine what modifications might logically follow, and the minimum amount of material was removed during each change. This modification of the same stator can be seen in Figures 18 through 23.

Runs 4 through 9 utilized Stator Configuration 1 with various modifications. The design clearances for stator one were 0.020" both axially and radially. Investigations during Runs 4, 5, and 6 were primarily concerned with developing operating procedures for starting and stopping the turbine and investigating the vortex patterns in the flow channels. For these runs, the front and back face stators were rotated so that corresponding parts were located 20°

from each other. The pressure taps on the front and back faces were connected to the Bourdon gages and recorded for verification with the predicted pressures in a well-formed water ring. The addition of stators effectively held the water ring around the rotors and resulted in a measurable increase in the torque absorption of the dynamometer.

As the turbine was started, a gradual closing of the water regulating valve resulted in the formation of the water ring and increased torque absorption. With the small radius of the dynamometer, closing the valve too rapidly resulted in driving the water ring in around the hub of the rotor, and water flowed from the adapter holes. A subsequent increase in turbine pressure ratio resulted in the expected RPM and torque increase and the water ring was pushed away from the hub by centrifugal force. The velocity build-up procedure can be accomplished much more rapidly in follow-on stator configurations of higher torque absorption capacity because it is not necessary to drive the water ring as close to the hub to appreciably increase the torque. Similar manipulation of the turbine air supply and the water regulating valve is required on shut-down to prevent flooding of the brake.

Run 6 was the first run in which a significant amount of energy was absorbed. The water inlet valve was manipulated during this run to determine the effect of reduced water inflow. The water inflow was reduced to about nine gallons per minute resulting in a slight decrease in the torque absorption. However, it was found that the inlet annulus must be kept full of water. Unsteady conditions result in the dynamometer if the water ring is unable to form equally around the periphery of the brake.

Runs 7, 8 and 9 utilized Stator Configuration 1, with the stator halves respectively: offset by 10^{o}, aligned, and aligned with an aluminum shim between the stators. The maximum usable turbine pressure ratio ($\frac{P_{to}}{P_2}$) was approximately 1.60 resulting in a power absorption of 31 horsepower at 7,060 RPM. An increase in pressure ratio above this value resulted in increased RPM without an appreciable increase in the torque absorption. Attempts to throttle the water to a greater extent caused leakage from the adapter holes. The power absorbed did not continue to be proportional to the cube of the RPM (Section IV). This occurred because there was not enough impingement area for additional torque absorption on Stator 1. Excessive turbulence in the wide channels destroyed the water ring and caused air-water foaming throughout the dynamometer. Operating conditions remained relatively steady. A 0.005" aluminum shim was used on Run 9 to divide the water exit channels in half in an attempt to reduce the formation of large vortices, for increased stability. No significant improvement resulted.

After reaching a desired turbine pressure ratio for each run, the water regulating valve was slowly opened at a constant pressure ratio to check the usable RPM range for a particular dynamometer configuration. Conditions became more unstable as the pressure holding the water ring around the rotor was decreased. Air pressure was introduced at the inner radius of the back face which had a slight stabilizing effect on the water ring. This occurred because the water regulating valve could be left in the same position, and the water ring could be pushed out by air pressure, thereby decreasing the torque.

Small tubes were installed between the high pressure outer-radius taps on the front face and the lower pressure taps at the inner radius

of the back face to determine whether the introduction of water to the back chamber would help to stabilize the water ring. Although water flowed readily through the tubing in the desired direction, no stabilizing effect was noticed.

Stator Configuration 2 was designed for Run 10. Fifteen radial slots were cut for water exit to the shroud. This number was selected in anticipation of additional modifications to either thirty or forty-five slots as required. Any of these configurations would result in an acceptable combination with the twenty-four rotor blades because of stability considerations. All other feasible numbers were considered, with emphasis on selection of a prime number of grooves, but none of these possible combinations could be as readily modified.

The axial and radial clearances for this stator were decreased to 0.015". Clearances of this order of magnitude were used for all subsequent runs and stator configurations. This clearance was considered to be a minimum when using plexiglass due to possible swelling upon heating. On early runs, care was taken to insure that the rotor was completely clear of the stator before starting the turbine. However, it was later found that a rotor-stator combination with slight rubbing could be readily worn-in with use, resulting in reduced clearances.

Run 10, Stator Configuration 2, relied essentially on disc friction and form drag for torque absorption, and very little torque was absorbed. Operating conditions were very steady due to the reduced free area throughout the brake.

At this stage in the development program it was recognized that a 20^{o} taper on the water regulating valve (2140-7, Figure 6) did not

permit sufficiently close control of the water ring. Also due to the small minimum diameter of the valve, it was necessary to close the valve by about half its total travel to get any appreciable regulating effect. The valve was redesigned with a 10^{o} taper, and machined from brass stock (Figure 7). Water exit flow was more closely regulated with the new valve, which was used for all subsequent runs.

The machining of thirty radial grooves 0.15" wide and 0.20" deep in the front and back faces modified Stator 2 to Stator 3 (Figure 19). The number of water exit slots was doubled to thirty. Run 11 with Stator 3 resulted in torque and power coefficients almost three times as large as with Stator 2. Although the torque absorption was not as high as with Stator Configuration 1, the operating conditions were very steady; and it was possible to operate at higher turbine pressure ratios and RPMs without causing break-up of the water ring.

It appeared that the major portion of the turbulent energy dissipation was occurring in the outer radius sections of the front and back face grooves, with very little vortex formation in the exit slots. An analysis of the velocity triangle diagram for the rotor exit conditions (Section 4) showed that water flow from the rotor, while it was turning at a high RPM, was nearly tangent to the blade. Therefore, the flow did not diverge sufficiently for an appreciable torque absorption area to be presented to the flow. The impingement area could be increased either by increasing the width of the radial slots or by cutting triangular pieces from the stator wedges preceding the slots. The latter design was selected because it resulted in more torque absorption area, better guidance of the flow to the area, and a large triangular space for vortex formation.

Half of the wedges were cut at a 30^{o} angle for Stator Configuration 4 (Figure 20). The close radial clearance on the rotor tips was thus still maintained through nearly half of the total periphery. The inner radius of the front face stator was beveled to increase the water inlet flow area and to help direct the incoming water into the rotor. Runs 12, 13 and 14 utilized Stator 4 which gave an increase in torque coefficient of 0.160.

Stator Configuration 5 (Figure 21) was machined by cutting the additional wedges at an angle of 30^{o}. On Run 15, the torque coefficient increased 0.157 over Runs 12 and 14 -- approximately the same increase that was noted when half the wedges were cut on a geometrically similar configuration (Runs 12-14 versus 11). For Runs 16 and 17, an aluminum shim that had been used between the stators to maintain the axial clearance was removed. Clearance with the rotor was thus reduced by 0.005" to a total of 0.010" and a slight increase in the torque-power coefficients was noted. It was observed on Run 17 that it was possible to close the water regulating valve to such an extent that turbulent mixing in the slots and grooves was visibly reduced. Opening of the valve, with the resulting decrease in case pressure, resulted in a slight increase in torque absorption and increased vortex formation in the grooves. Further opening of the valve caused the water ring to move out and the torque absorption to decrease in the normal manner. Thus, it appeared that it was not advantageous to attempt to pressurize the water ring to a greater extent than was required to hold the ring in place against centrifugal force. Increased torque absorption resulted on Run 18, using slightly reduced throttling.

Acceptable stability for turbine tests over a velocity range of approximately 5,000 RPM at all turbine pressure ratios resulted with Stator Configuration 5. The torque absorption characteristics nearly equalled the minimum required goal of the development project, and data obtained using this configuration correlated well with the data obtained using the air dynamometer. Instability above the operating range occurred because close radial clearances were maintained over only a small percentage of the total periphery in Stator 5, and considerable foaming occurred outside the blades. Upon disassembly, excessive wear was noted on the thin sections that were maintaining the radial clearance, although these sections had been machined 0.15" wide instead of coming to an acute angle as in Figure 21. It is assumed that similar wear would occur with time on stainless steel stators because of the excessive turbulence and torque absorption in these areas.

To increase the torque absorption above the minimum goal curve, the stator was modified to Stator Configuration 6 by cutting the face grooves deeper to 0.25" and angling them 45° in the direction of rotation. Thus water entering the slots was turned through an angle 45° greater than with non-angled grooves, leading to increased momentum transfer. Upon exiting the grooves, the flow was directed backwards against the oncoming blades, also increasing the energy required to accelerate the flow in the direction of rotation. A considerable increase in torque absorption resulted, but the operation was slightly more unsteady than during previous runs, upon attempting to decrease the torque.

The rotor diameter, the characteristic dimension of the dynamometer, has a large effect on the torque absorption of the brake. Two rotors of 6.5-inch diameter and 0.220" thickness were designed with a profile similar to that shown in Figure 14. The 6.5" diameter rotors were the largest rotors that fit in the casing and still allowed space for a radial stator to be located between the rotor and the shroud. They were arranged in Rotor Configuration 2 (Figure 11) and tested in Run 20. Configuration 6 was cut to the larger diameter for use as the front and back face stators. For Run 20, no stator was placed in the slot between the two rotor blades. Very steady operation and increased torque resulted with maximum throttling, but upon slowly opening the water regulating valve and decreasing the pressure on the water ring, water apparently poured into the space between the rotors, and the turbine accelerated rapidly.

Stator Configuration 7 (Fig. 24) was used for the back face stator for Runs 21 to 26. This stator was machined with the face grooves angled 45^{o}. The grooves were not cut all the way to the hub in an attempt to prevent water leakage from the adapter holes when using a maximum torque setting.

For Runs 21 and 22, a slotted 0.15" thick stator (Figure 25) was located between the rotors. In essence, this made the dynamometer a two-stage machine of similar geometry to Run 20. The torque and power coefficients almost doubled. One explanation for the fact that they did not double exactly is that there was no way to angle the stator grooves on the mid-stator for exact geometric similitude. A small amount of air pressure was introduced at two taps on the back face to stabilize the operation. A difficulty encountered with the high

torque stator configurations was that the RPM of the turbine could be considerably decreased, but upon opening the water regulating valve, the operation would become unsteady before reaching the minimum RPM which had been obtained with the air dynamometer for a particular turbine pressure ratio. To decrease the torque absorption, an uncut flat stator was placed between the blades for Run 23. However, when the water ring was not closed down near the hub, insufficient cooling water circulated between the front and back chambers, and cavitation occurred in the back chamber.

A rotor plate of 6.5" diameter similar to Figure 15 was located between the rotors for Runs 24 and 25. This was designated as Rotor Configuration 3 (Figure 11). The resulting torque coefficient was approximately equal to that of Run 23. This may be a coincidence or it may indicate that geometrically similar arrangements formed by either mid-rotor stators or mid-rotor blank-off plates turning with the rotor yield the same torque absorption. This is an area for further investigation. For Runs 26 to 28, the two rotors were placed together giving a cross section similar to Configuration 1 but with increased diameter. For Run 26 the torque absorption was approximately the same as for Runs 23 to 25. The back face stator that had been used earlier (Runs 19 and 20) with the face grooves cut all the way to the hub was installed for Run 27 in order to test a machine more geometrically similar to Run 19. As expected, slightly lower torque absorption occurred (Section V).

It was extremely difficult to decrease the torque during Runs 23 to 26 in small increments. After approximately 500 RPM increase, excessive foaming would occur. The water ring would jump outside the

rotor and the rotor would accelerate to approximately 10,000 RPM. Various combinations of air pressurization, decreasing the water inlet flow, and varying the water regulating valve had little effect. It appeared that these configurations did not allow enough water exchange between the front and back sections of the brake to automatically prevent surging by allowing water to flow to areas of reduced local pressure.

A stator configuration similar to Figure 19, cut to accommodate the 6.50" diameter rotor, was tested on Run 28. This was considered to be the optimum water brake configuration for the required torque absorption and stable operating conditions. This configuration was machined from stainless steel (SS 301) upon completion of the development process.

IV. ANALYSIS OF THE WATER DYNAMOMETER

A. DIMENSIONAL ANALYSIS

A dimensional analysis of the water dynamometer was utilized to identify the significant operating parameters of machines of this type. This method has general application in the analysis of all turbomachines. Additional information on this method and physical similitude can be found in Shepherd [Ref. 6]. Mass (M), length (L), and time (T) were chosen as the primary dimensions. In this system, force (F) is proportional to ML/T^2.

The parameters that were selected as being of primary interest in the dynamometer were:

Symbol	Dimensions
Q - Water volumetric flow rate	- L^3/T
P - Power absorbed	- ML^2/T^3
N - Revolutions per minute	- $1/T$
D - Characteristic Dimension	- L
ρ - Density of the working medium	- M/L^3
μ - Absolute viscosity of the working medium	- M/LT
H - Energy per unit mass or "head"	- L^2/T^2
τ - Torque (a known function of power and RPM, but of particular interest in this investigation)	- ML^2/T^2

Additional fluid properties such as elasticity and surface tension were not considered in the analysis but may be of importance in other applications.

There are eight selected parameters and three primary dimensions. Hence five dimensionless coefficients can be found which must have a bearing on the performance of the dynamometer.

A kinematic variable - N, a geometric variable - D, and a fluid property - ρ, were selected as primary because together they contain all the primary dimensions, do not form a dimensionless product, and appeared to be capable of manipulation as variable performance parameters. A dimensionless coefficient called the power coefficient K_P is obtained in the following manner:

$$K_P = f(N, D, \rho, P)$$

$$K_P = \left(\frac{1}{T}\right)^a (L)^b \left(\frac{M}{L^3}\right)^c \left(\frac{ML^2}{T^3}\right)^1 = M^o L^o T^o$$

The three simultaneous equations for M, L, and T are,

for M: $c + 1 = 0$

for L: $b - 3c + 2 = 0$

for T: $-a - 3 = 0$

Thus:

$a = -3$ $\quad b = -5$ $\quad$ and $\quad c = -1$

and:

$$K_P = \frac{P}{N^3 D^5 \rho}$$

The other coefficients are obtained in a similar manner, namely:

Torque Coefficient $\quad K_\tau = \dfrac{\tau}{N^2 D^5 \rho}$

Flow Coefficient $\quad K_Q = \dfrac{Q}{ND^3}$

Viscosity Coefficient $$K_{\mu} = \frac{\mu}{ND^2\rho}$$

Head Coefficient $$K_H = \frac{H}{N^2D^2}$$

The power coefficient K_P is sometimes called the "machine constant" [Ref. 1]. With the dimension D chosen as the rotor diameter, the product ND is proportional to the linear velocity of the rotor. This is called the blade speed and is usually denoted by U.

Hence

$$D^3N^3 \alpha U^3$$

and

$$P = \text{Power} = K_P \rho D^5N^3 \alpha K_P \rho U^2D^2U$$

The quantity ρU^2 has the dimensions of a pressure.

Then

$$P \alpha K_P \Delta p D^2U$$

Similarly

$$\tau = \text{Torque} = K_\tau \rho D^5N^2 \alpha K_\tau \rho U^2D^3$$

$$= K_\tau \Delta p D^3$$

The torque coefficient can be shown to be proportional to the power coefficient

$$K_\tau = \frac{\tau}{N^2D^5\rho} = \frac{\tau}{N^2D^5\rho} \left(\frac{N}{N}\right)$$

For τ in ft-lbf, P in $\frac{\text{ft-lbf}}{\text{sec}}$

$$P = \tau\omega = \frac{\tau 2\pi N}{60} = \frac{\pi}{30} k_\tau N^3 \rho D^5 = K_P\rho D^5N^3$$

Therefore

$$K_\tau = \left(\frac{30}{\pi}\right) K_P$$

Hence K_P and K_τ are equal except for a constant or

$$\frac{K_P}{K_\tau} = \text{constant.}$$

The characteristic dimension D has previously been assumed to be the rotor diameter, but from the development of the power coefficient in terms of pressure, and from experiments with geometrically similar machines [Ref. 6], it has been shown that D^5 in K_P is the product of two dimensions representing the cube of the rotor diameter and a flow area. Attempts to define the relationship by putting two or three different dimensions in the analysis lead only to ratios of the dimensions. Experiments are required to determine their relationship to each other and which dimensions are important in a particular machine.

The flow rate

$$Q = \text{Fluid velocity (V) X Flow Area}$$

$$Q \propto VD^2$$

Therefore $K_Q = \frac{Q}{ND^3} \propto \frac{V}{ND}$

again, since ND is proportional to U,

$$K_Q \propto \frac{V}{U}$$

V/U is the ratio of fluid velocity and blade speed. Thus a particular velocity triangle is a significant parameter of the water dynamometer. Similar velocity triangles would result for various values of Q, N, and D, if the flow coefficient K_Q were constant.

In a similar manner

$$K_H = \frac{H}{N^2 D^2} \alpha \frac{H}{U^2}$$

U^2 is a rotor kinetic energy term. The ratio of fluid head to kinetic energy is thus seen to be a significant parameter. This factor is considered in the design differences between a pump and a water dynamometer as discussed in Section C.

Since $\frac{V}{U}$ is constant for similar conditions

$$K_H \alpha \frac{H}{U^2} \alpha \frac{H}{V^2} \alpha \frac{H}{UV} .$$

Expressing the head H as $\frac{\Delta P}{\rho}$

$$K_H \alpha \frac{\Delta p}{\rho V^2}$$

Thus, K_H is a basic ideal fluid flow characteristic.

The viscosity coefficient is similar to a Reynold's number for the dynamometer, or

$$K_\mu = \frac{\mu}{ND^2\rho} \alpha \frac{\mu}{UD\rho} \alpha \frac{\mu}{\rho VD}$$

This could be a significant parameter in comparing machines utilizing different working fluids.

Additional dimensionless coefficients can be formed from combinations of the coefficients previously found to be of significance. For example, in some applications where the flow rate (Q) and the energy per unit mass (H) can be varied to a significant extent, a dimensionless variable not containing a characteristic length can be formed as follows:

$$K_6 = \frac{(K_Q)^{1/2}}{(K_H)^{3/4}} = \left(\frac{Q^{1/2}}{N^{1/2}D^{3/2}}\right)\left(\frac{N^{3/2}D^{3/2}}{H^{3/4}}\right) = \frac{NQ^{1/2}}{H^{3/4}}$$

This coefficient is usually called the specific speed, N_s, and would be characteristic of geometrically similar machines of all sizes. In typical machines, N_s varies over a wide range of values, but where it is evaluated at the maximum efficiency point, it becomes a significant machine parameter [Ref. 6].

For the water dynamometer, the only variables that could be varied to a significant extent were the rotor RPM, the rotor diameter, and the machine constant K_P. A particular stator-rotor configuration is characterized by a distinct value of the machine constant under maximum torque conditions. For a stable water ring, a geometrically similar configuration of larger diameter would be capable of minimum power absorption

$$P = K_P \rho N^3 D^3.$$

This formula uses the conservative estimate of power absorption based on the cube of the rotor diameter instead of the fifth power. The characteristic flow area is assumed to be constant. It may actually be a rotor periphery times width, a rotor area, or a typical water inlet or exit area. Further experimentation utilizing several different rotor diameters in geometrically similar configurations is required to determine which of the flow areas is characteristic and what are its functional relations with the rotor diameter. This question is discussed in Section V.

B. DISC FRICTION ANALYSIS

The following presents the calculation of the disc friction drag on a flat rotor rotating in a housing. It must first be determined whether the flow is laminar or turbulent. Water at 70° F was assumed to be the medium. The rotor radius was taken as 2.75". The analysis was made for the rotor turning at 10,000 RPM. With the kinematic viscosity $\nu = \frac{\mu}{\rho}$, the Reynold's Number is

$$R_N = \frac{R^2\omega}{\nu} = 5.2 \times 10^6$$

where R is the radius of the rotor. The flow is turbulent above $R_N = 3 \times 10^5$ for flow near a rotating disc, so the water brake operates in the turbulent regime. Due to friction on the rotor, fluid in the immediate vicinity of the disc is carried along by the disc and forced outward by centrifugal acceleration. The general circulation pattern in the water brake is outward along the rotor and toward the hub along the faces. The central core rotates at an average angular velocity that is about half the velocity of the disc.

An expression for the turbulent boundary layer thickness was found by balancing the viscous and centrifugal force expressions [Ref. 5].

$$\delta_T = .526 \left(\frac{\nu}{r^2\omega}\right)^{1/5} \cong 0.0004 \text{ " at the maximum radius.}$$

r is rotor radius at the point in question. The casing of the dynamometer was well outside the turbulent boundary layer even when a stator of close clearances was utilized.

The dimensionless moment coefficient C_M, which is proportional to the torque coefficient, is defined as

$$C_M = \frac{2\tau}{\frac{1}{2}\rho\omega^2 R^5}.$$

for a disc wetted on both sides. For a disc rotating in a casing with walls outside the boundary layer, in turbulent flow, Schultz-Grunow [Ref. 5] found an approximate expression for the moment coefficient

$$C_M = .0622\ (R_N)^{-1/5}$$

Thus

$$\tau = \frac{C_M}{4} \rho \omega^2 R^5 \cong 45.33 \text{ IN-lbf for the water brake at 10,000 RPM}$$

Experiments have shown that the Schultz-Grunow expression leads to torque values that are about 17% too low due to assumptions made in the calculations. When a correction is added to the value above, the torque absorption in the water brake solely from frictional effects on a flat disc of 5.5"D becomes 53.02 IN-lbf at 10,000 RPM.

C. CENTRIFUGAL PUMP VERSUS WATER BRAKE DESIGN

In Section A, manipulation of the head coefficient showed that the ratio of fluid head to kinetic energy is a significant parameter. In general, a centrifugal pump is designed to optimize the pressure increase across the pump at relatively high flow rates. Increased efficiency results when the absolute velocity leaving the rotor is as small as possible. This velocity is then converted into pressure head in a well-designed diffusor. Blades canted opposite to the direction of rotation are typical of centrifugal pumps. This reduces the absolute velocity (V) as seen in the velocity diagram of the pump.

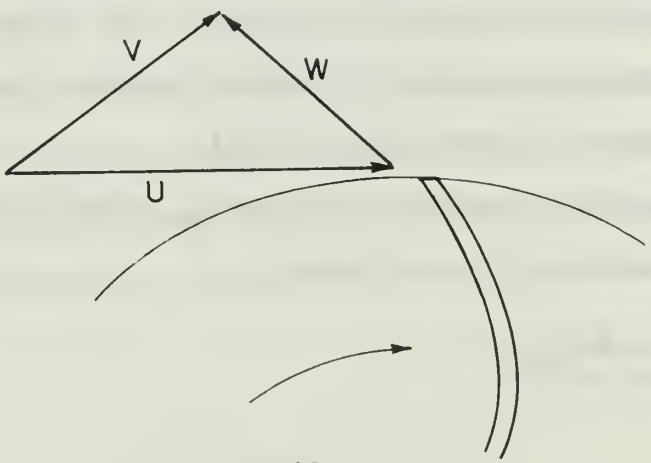

where W = the relative velocity of flow leaving the rotor

V = the absolute velocity of the flow

U = the blade speed = ωR

The degree to which the blades can be canted backwards is limited by the blade stresses under centrifugal force and the requirement that a finite outlet velocity is required to maintain flow through the pump.

Conversely, a water brake is designed to be as inefficient as possible so that the maximum energy is absorbed. This can be accomplished with forward canted blades resulting in a large absolute velocity leaving the rotor. The velocity is then rapidly decreased upon impingement on a stator, imparting turbulence to the flow. The kinetic energy of the flow is inefficiently converted to a temperature rise in the fluid and a reduced pressure rise.

The velocity diagram is:

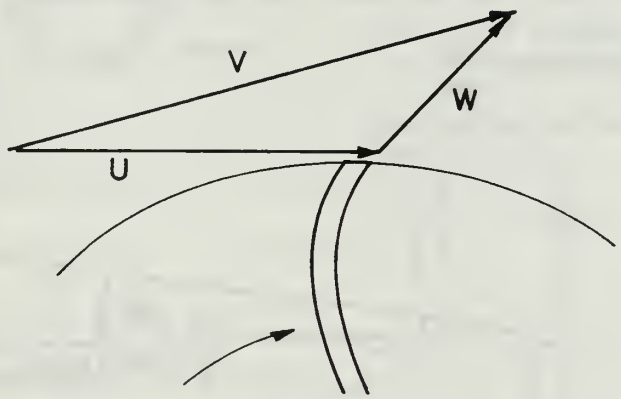

Both the blade stresses that result at high RPM and machining considerations, dictated the selection of straight radial blades for the water dynamometer.

The rectangular cross section of the blades increases the form drag torque absorption compared with the drag that would result with airfoil shaped blades. The sharp edges of the rotor blades cause the

separation point to remain fixed at the corner resulting in steady operating conditions. The sharp-edged blade design also increased the turbulence in the wake of the blades. The requirement for increased torque absorption from Stator Configuration 3 (Figure 19) led to an analysis of the velocity diagram at a mid-range operating condition of 6,000 RPM and 12 gallon/minute water flow rate.

The total water exit flow area was assumed to be the number of radial slots times the area of one slot. Larger areas with increased flow rates are perhaps more representative of conditions due to the circulation pattern in the brake, but the increased flow rate and flow area may result in the same relative velocity leaving the blade. When the maximum possible energy was being absorbed, the internal circulation pattern did not appear to extend to the tips of the rotor blades due to pressurization of the water ring.

The water flow area (A) was 0.017 ft^2 for Stator 3.

$$W = \frac{Q}{A} = 1.56 \frac{ft}{sec}$$

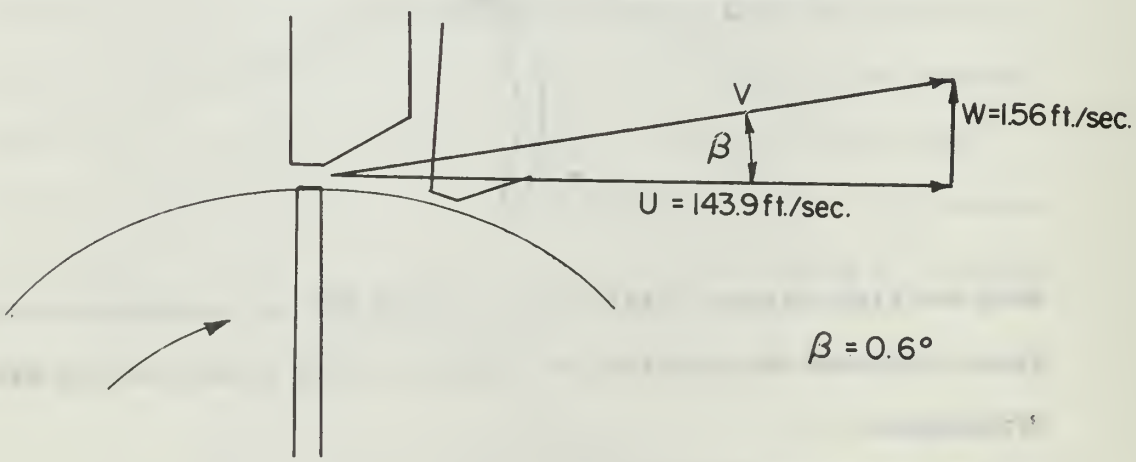

β is the divergence angle of the flow measured with respect to the tangent to the rotor blade.

For angular velocities between 4,000 and 10,000 RPM and water flow rates between 9 and 13 gallons/min, the divergence angle (β) was not greater than 1.5^{o}. Triangular wedges were cut from the stator to increase the flow impingement area for greater torque absorption. This enabled the flow to diverge over the entire distance from the beginning of the cut to the next stator section. A wedge angle of 30^{o} was used to increase the area for turbulent mixing and vortex formation after impingement.

D. PRESSURES IN A ROTATING MEDIUM

A determination of the pressures in a rotating medium caused by centrifugal force was required for stress calculations on the dynamometer components. A comparison of observed to predicted pressures was used to determine whether a solid water ring was forming properly in the brake.

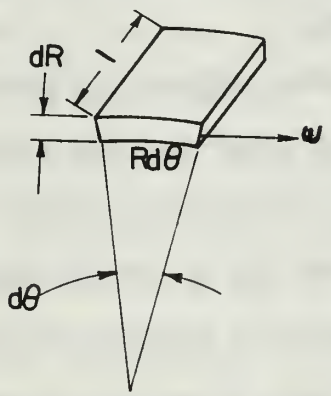

The axial length of the particle is taken as unity.

The volume of an elemental particle is

$$dV = Rd\theta \; dR \quad (1)$$

$$dm = \rho dV = \rho Rd\,\theta dR$$

Centrifugal Force balance $F_c = m.a$

$$F_c = dm\,\omega^2 R = \rho Rd\theta dR\omega^2 R = \text{Area } (dP) = Rd\theta dP$$

where dP = the change in pressure across the elemental area

and Area = the area upon which the centrifugal force (F_c) acts = $Rd\theta(1)$

Thus $dP = \rho\omega^2 RdR$

This equation can be integrated between an inner radius R_i where the pressure is known or assumed and the radius R_o in question, to determine the pressure increase in the water ring.

$$\Delta P_{(R_i \text{ to } R_o)} = \frac{\rho \omega^2 R_o^2}{2} - \frac{\rho \omega^2 R_i^2}{2}$$

It was found that under normal operating conditions, the gage pressure at R_i = 1.75", the inner radius of the rotor teeth, was nearly zero. The angular velocity (ω) of the water ring was used for calculations. The water ring was assumed to rotate at half the velocity of the rotor. With the rotor turning 10,000 RPM, a gage pressure of 97.4 psi is predicted at a radius of 3.25".

Pressure differentials observed on the Bourdon gages during the runs were very close to the predicted values under maximum torque absorption conditions. The observed pressures dropped considerably if the water regulating valve was opened to decrease the torque, and if foaming developed in the water ring.

It was possible to increase the water pressure throughout the dynamometer by increased closure of the water regulating valve. As increased pressure at the water inlet station was observed however, the pressure differential from the rotor hub to the tip remained the same. It was found to be disadvantageous to increase the chamber pressure in this manner, because turbulent mixing in the brake was retarded.

E. THE OPERATING ENVELOPE OF A WATER DYNAMOMETER

The typical operating envelope of a water dynamometer is discussed in Ref. 1 and shown on the next page.

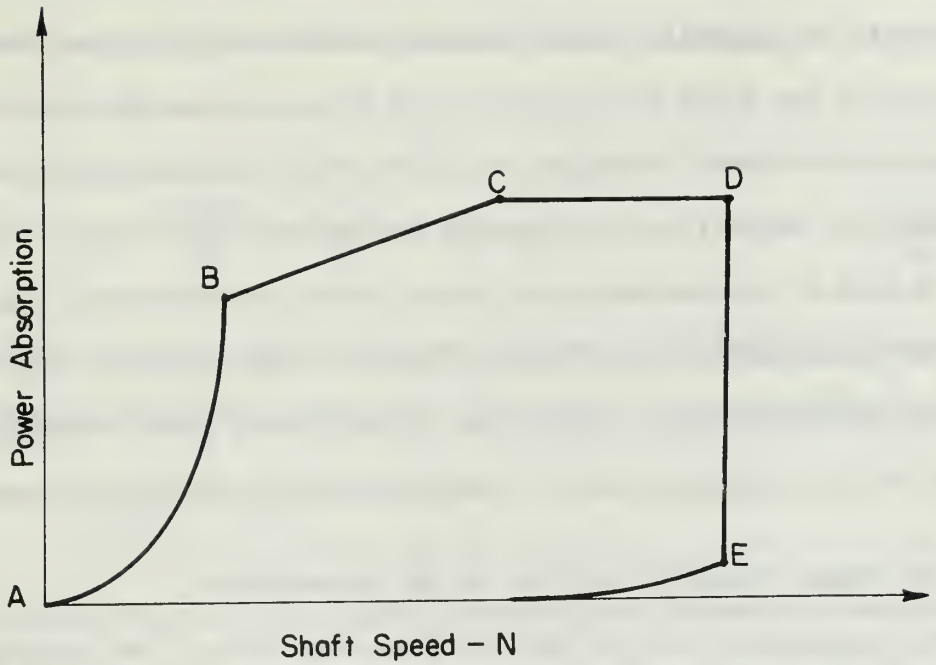

At low RPM, the maximum power that can be absorbed is a function of the machine constant of the dynamometer configuration and a certain power of the rotor diameter. The curve A to B rises as the third power of the RPM. In the typical machine, at point B, the torque has risen to the stress limit of the rotor shaft, and increased power absorption from B to C must be linear with shaft speed (Power $\alpha N \tau_{max}$). In the water dynamometer of this report, point B was limited in early stator configurations by the small impingement area of the stator. In later configurations it was limited by the maximum power output of the TTR when operated in the unhooded configuration [Ref. 3]. Even when the TTR is run in a hooded configuration at higher turbine pressure ratios, the water brake is capable of absorbing sufficient power to limit the RPM to the range of interest, because lower mass flow rates through the TTR are utilized resulting in power outputs of the same order of magnitude as in unhooded operation.

Line C-D is a constant maximum power absorption line. This represents the capacity of the machine to remove the thermal energy imparted to the fluid by the rotor. It is determined by the cooling capacity of the heat exchanger or in the water dynamometer by the maximum cool water flow rate through the machine (See Section IV F). Line D to E is the maximum shaft speed for the rotor-turbine combination as determined by centrifugal stresses. This limit is 20,000 RPM for the TTR-water brake. Curve E-A is the lowest power absorption level of the dynamometer due to bearing friction and other losses.

F. THE ENERGY TRANSFER ANALYSIS IN THE DYNAMOMETER

The temperature rise in the fluid passing through the dynamometer at a known water flow rate can be used as an alternate method of determining the power absorbed in the brake. It is also necessary to determine the temperature rise of the fluid in the dynamometer in order to prevent cavitation. A larger heat exchanger or increased water flow rate would be required to prevent cavitation if the temperature were increased to such an extent that the case pressure would become smaller than the fluid vapor pressure at that temperature. External heat transfer to or from the fluid as it passes through the dynamometer is assumed to be negligible. The weight flow rate through the dynamometer is

$$\dot{w} = \rho g Q \qquad \frac{\text{lbm}}{\text{sec}}$$

The energy input to the fluid from the shaft is

$$E_S = \frac{\tau \omega}{\dot{w}} \qquad \frac{\text{ft-lbf}}{\text{lbm}}$$

The energy gained by an incompressible fluid between the water inlet (station 1) and the outlet (station 2) for an adiabatic process can be expressed as

$$E_G = \frac{p_2 - p_1}{\rho g} + \frac{V_2^2 - V_1^2}{2g} + (Z_2 - Z_1) \qquad \frac{\text{ft-lbf}}{\text{lbm}}$$

The velocities at station (1) and (2) are equal from the incompressible continuity equation because the flow areas are approximately the same.

$$\rho_1 A_1 V_1 = \rho_2 A_2 V_2$$

The geopotential energy change is also zero because the water entrance and exit are at approximately the same height. For a pressure increase from station 1 to 2 of 100 psi (the dynamometer acting as a centrifugal pump)

$$E_G = .296 \frac{\text{BTU}}{\text{lbm}}$$

This is negligible compared to the energy input from the shaft which is primarily converted into a temperature rise of the water.

$$E_H = E_S - E_G$$

where E_H is the absorbed energy that heats the fluid.

$$E_H = C_p (\Delta T_W)$$

$$\Delta T_W = \frac{E_H}{C_p}$$

ΔT_W is the temperature rise (^oF) of the water.

The water temperature is increased by 66.2^oF in passing through the dynamometer at a flow rate of 9 gallons per minute when operating at the power absorption goal of 117 HP.

G. THE WORKING FLUID ANALYSIS

The optimum working fluid for machines of this type would have a high density to increase the form drag, disc friction drag, and momentum transfer. It must also possess a relatively low kinematic viscosity so that the fluid flows easily to all parts of the brake and is readily pumped through the brake passages. Other desirable features include a large specific heat, high boiling point, and low vapor pressure for increased energy absorption without the problems associated with the occurrence of cavitation. The corrosion characteristics and toxicity of the fluid should also be considered. For the open system described in this report, water proved to be the most practical fluid to use. For other applications, a water-glycol mixture, or a high density hydraulic fluid may be more suitable. The closed system described in Ref. 1 utilized a fire resistant heat transfer fluid.

H. DATA REDUCTION

For all the water dynamometer test runs, the TTR was operated as an impulse turbine with the double circular-arc rotor blades with sharp leading edges described in Ref. 3. The stator had converging nozzles. The rotor axial clearance was 0.250 inches, and the radial clearance was 0.009 inches for all of the tests.

For many of the runs where only the water dynamometer performance was of interest, hand calculations of the significant parameters were made. The torque output reading was converted to torque (in-lbf) with the calibration curve (Figure 10). The RPM was recorded directly from the electronic counter in the control room.

The power absorbed by the dynamometer is

$$P \alpha \tau N$$

$$= (\tau \text{ in-lbf}) \left(\frac{\text{ft}}{12 \text{ in}}\right) \left(\frac{N \text{ REV}}{\text{min}}\right) \left(\frac{2\pi \text{ Rad}}{\text{REV}}\right) \left(\frac{\text{MIN}}{60 \text{ sec}}\right) \left(\frac{\text{HP-sec}}{550 \text{ ft-lbf}}\right)$$

$$P = \tau N \ (.00001587)$$

This is the power output of the turbine if the small dynamometer and rotor bearings losses are ignored.

The turbine pressure ratio $\left(\frac{P_{to}}{P_2}\right)$ is the ratio of total turbine inlet pressure and ambient atmospheric pressure for unhooded operation. The turbine exit pressure (P_2) is the atmospheric pressure in the unhooded operation. The pressure ratio was computed directly from the mercury manometer board readings by converting P_{to} to absolute pressure (in-Hg) from the board atmospheric reference reading and the control room barometer reading.

The water inlet and exit thermocouple readings in millivolts were converted to temperatures (^{o}F) from tables of the Iron-Constantan millivolt readings at 0^{o} reference temperature. An ice-water bath was used for the reference junction. The water ring pressures were recorded directly from the Bourdon gages. The water flow rates were calculated by allowing the exit water to flow into a barrel for weighing. The weight of water collected in a minute was converted to gallons per minute.

$$\dot{w} = \left(\frac{\Delta w\text{-lbs}}{\text{MIN}}\right) \left(\frac{\text{gal } H_2O}{8.345 \text{ lb}}\right) \qquad \text{(GPM)}$$

The significant parameters were converted to the ft-lb-sec system for calculating the torque and power coefficients. This yields non-dimensional torque and power coefficients that are equal and that can

be compared with consistent dimension coefficients in any other system. However, consistent units are not required for the comparison of coefficients between different runs. Horsepower, RPM, density in lbm per cubic feet, etc. could be used directely, and the coefficients calculated would differ by a constant factor from those of the ft-lb-sec system. For the rotor diameter to the fifth power analysis.

$$K_P = \frac{\text{Power}}{N^3 D^5 \rho} = \frac{(HP)(550\ \frac{\text{ft-lbf}}{\text{sec HP}})}{(\frac{\text{REV}}{\text{MIN}})^3 (\frac{2\pi\text{Rad}}{\text{REV}})^3 (\frac{\text{Min}}{60\ \text{sec}})^3 (D(\text{in}))^5 (\frac{\text{ft}}{12\ \text{in}})^5 (\frac{\rho\text{-Slugs}}{\text{ft}^3})}$$

$$= \frac{HP}{N^3 D^5} (61,427,539,713.6) \quad \text{for water}$$

Similarly

$$K_\tau = \frac{\text{Torque}}{N^2 D^5 \rho} = \frac{\tau}{N^2 D^5} (974,684.23) \quad \text{for water}$$

When using this consistent system of units

$$K_\tau = K_P$$

For the analysis based on the cube of the rotor diameter, a constant flow area of one square inch was used in the denominator to determine the coefficients. In a similar manner, a flow area of one inch times the rotor diameter in inches was used in the denominator for the fourth power analysis.

For some water brake runs a complete set of turbine data was recorded for comparison with the turbine performance using the air dynamometer. This data was reduced on the IBM 360/67 computer of the Naval Postgraduate School using the program developed by Esdaile [Ref. 4]. Figure 28 shows the extension of operating range made

possible by the development of the water dynamometer. The total-to-static turbine efficiency (η_{ST}) is the ratio of actual power produced by the turbine stage and the theoretical turbine power determined by the air flow rate ($\frac{lbm}{sec}$) through the turbine and its isentropic enthalpy drop (Δh_{is}) from total turbine inlet conditions to static pressure at turbine discharge. The kinetic energy of the absolute exit velocity is considered to be lost in the determination of total to static efficiency.

$$\eta_{ST} = \frac{HP\ (550)}{\Delta h_{is}\ \dot{w}J} = \frac{\tau\omega(\frac{1}{12})}{Cp\Delta T_{is}\dot{w}J}$$

The isentropic temperature drop (ΔT_{is}) across a turbine state is

$$\Delta T_{is} = T_{to}\left[1 - (\frac{P_2}{P_{to}})^{\frac{\gamma-1}{\gamma}}\right]$$

where T_{to} is the total temperature before the stage and $\frac{P_2}{P_{to}}$ is the inverse of the turbine pressure ratio.

The program uses the NASA reference system to refer the flow rate, rotational velocity, dynamometer moment, and horsepower to standard air conditions as follows:

$$W_{REF} = \frac{\dot{w}\sqrt{\theta}}{\delta}$$

$$N_{REF} = \frac{N}{\sqrt{\theta}}$$

$$\tau_{REF} = \frac{\tau}{\delta}$$

$$HP_{REF} = \frac{HP}{\delta\sqrt{\theta}} = \frac{\tau\omega}{550(12)\,\delta\sqrt{\theta}}$$

with

$$\theta = \frac{T_{to}}{518.4}$$

$$\delta = \frac{P_{to}}{14.7}$$

V. DISCUSSION OF RESULTS

The primary goal of this project was to develop a water dynamometer with the operating characteristics required for turbine tests at the Turbo-Propulsion Laboratory. Due to modifications to the stators in the development process, no two machines of different radius with exact geometric similarity had been tested upon the completion of Run 26. However, Run 26 with the increased diameter rotor was basically the same configuration as Run 11 except that the grooves in the faces were angled 45^{o} on Run 26. Run 26 also used a configuration similar to Run 19, except that Run 19 had 30^{o} wedges cut in the stator around the tips of the rotor blades.

All calculated K_P values are considered to be the approximate machine constants of each rotor-stator configuration. All the values are based on a maximum torque setting for each run and are dependent on the degree to which the water ring was closed down around the hub of the rotor. For the machine described in Ref. 1, it was found that the machine constant was not a constant, but in fact had a strong dependence on Reynold's number. The machine constants for the water dynamometer increased slightly with increased turbine pressure ratio (Table A1). It is felt that this occurred primarily because it was necessary to pressurize the water ring to a greater extent to hold the ring around the rotor with increased shaft power input. The power absorption has previously been shown to be pressure dependent.

In an attempt to determine the relationship between the characteristic dimensions of flow area and rotor diameter, the machine constants K_P of each configuration were calculated based on the cube, fourth

power, and fifth power of the rotor diameter respectively. A constant flow area was assumed for the diameter cubed analysis, and a constant length times the diameter was used for the flow area for the fourth power analysis. The calculated machine constants are listed in Table A1.

With the three different methods, the increase in K_P caused by cutting the 30^o radial wedges was determined by calculating $[K_{P\ (Run\ 15)} - K_{P(Run\ 11)}]$. For Runs 12 and 14 only half the wedges were cut, and the K_P increase was half of the total increase. The above listed term was subtracted from the K_P of Run 19 to yield a predicted value for Run 26. In a similar manner, the increase in K_P caused by cutting the face grooves at a 45^o angle was determined from $[K_{P\ (Run\ 19)} - K_{P(Run\ 17)}]$. This K_P increase was added to the K_P of Run 11 to yield another predicted value for K_P of Run 26. These two methods gave approximately the same value for K_P and the mean was used for the "predicted K_P - Run 26-27" line of Table A1. The predicted machine constant was lower than the actual K_P of Run 26 by 39%, 28%, and 14%, respectively, for the three different rotor diameter analyses. A slight increase in the coefficient for Run 26 can be accounted for by the fact that a new back stator design (Figure 24) was used for Runs 21 through 26. Run 27 utilized the original back stator design of Run 19 with the water grooves cut all the way to the stator hub. The power coefficients decreased slightly as expected for the three methods of analysis. The power coefficient based on the fifth power of the rotor diameter was slightly lower than the predicted value. This was anticipated because the 6.50" diameter rotor is slightly thinner in the axial direction than the 5.50" diameter rotor.

Pending further experiments utilizing geometrically similar configurations with rotors of several different diameters, it appears that using the fifth power of the rotor diameter as the characteristic dimension is the most suitable method for extending the test results to larger diameter machines. It was also noted that this method was the only one of the three that gave a lower overall machine constant for Runs 26-27 than for Run 19 as would be expected with the simplified stator arrangement of Runs 26-27.

All the runs from 19 to 27 showed a degree of unsteadiness upon attempting to decrease the torque absorption. Stator configurations with angled face grooves were used on all of these runs. With several of the configurations, the RPM increased rapidly at a point approximately 500 RPM above the maximum torque absorption RPM, and it was impossible to set and maintain intermediate RPM conditions. It was surmised that the reason for this was that with the angled grooves and sharp-edged rotors, a slight velocity increase caused a change in the internal flow pattern of the brake. Normally, water leaving the grooves impinges on the flat faces of the rotor and increases the form drag effects. However, as the RPM is increased, the relative flow angle with respect to the plane of rotation of the rotor becomes smaller. A reduced impingement area results, and an increased percentage of the flow may be directed to the side of the rotor. Conditions would be unstable because a small RPM rise would be self propagating, leading to a rapid increase in the RPM.

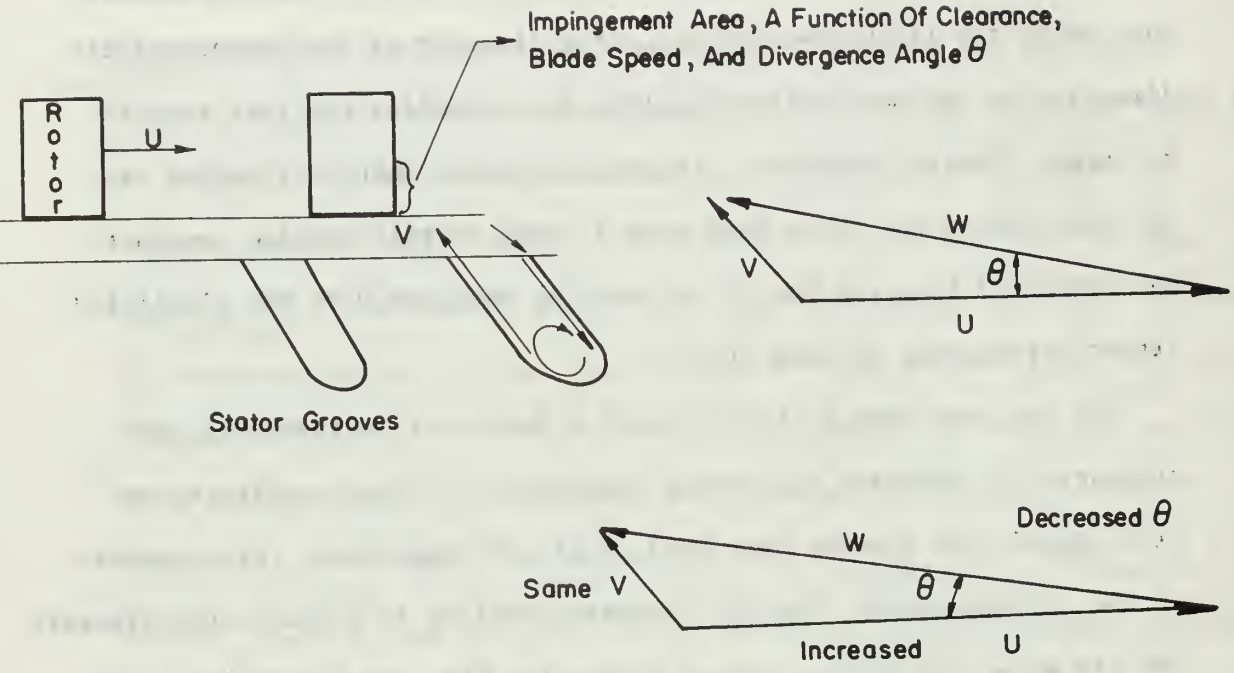

The absolute velocity V leaving the stator is assumed to remain about the same for the original small RPM increase at constant torque. Actually, with increased rotor velocity, the amount of flow entering the grooves may also decrease for similar reasons, and the absolute velocity and water flow rate leaving the grooves may decrease, decreasing the relative flow angle to an even greater extent.

The torque absorbed in the later runs was considerably higher than required for the majority of the investigations to be conducted at the Turbo-Propulsion Laboratory. The plexiglass stators are available for individual runs where very low RPM is a requirement. However for general use, a stator arrangement similar to Figure 19 (Run 11) using a rotor of 6.50" diameter was considered to be the optimum design with respect to required power absorption and steady operating conditions. Even with the conservative estimate of using the rotor diameter to the third power to extend the torque absorption characteristics of Run 11

to the larger machine, it was predicted that a machine with this configuration would be capable of absorbing 119.74 HP at 10,000 RPM. If the rotor diameter to the fifth power analysis were correct, the machine would absorb 167.54 HP.

This configuration was utilized for Run 28 and the power coefficient based on the fifth power of the rotor diameter was approximately the same as the coefficient for Run 11. This helps to verify the fifth power method of analysis for water dynamometers of this type. The power absorption was well above the minimum required, and stable operating conditions prevailed to an RPM at which the air dynamometer can be used.

VI. CONCLUSIONS AND RECOMMENDATIONS

A water dynamometer with acceptable stability and accuracy for the testing of small gas turbines was developed. It is capable of absorbing considerably more energy than required as a minimum goal of this project. The dynamometer expands the useful operating range of the turbine for investigations at off-design and starting conditions and augments the capability of operating the TTR at transonic and supersonic rotor entrance velocities. The extension of the usable RPM range is shown in Figure 28. The flow characteristics in machines of this type were investigated and the primary problem areas were identified.

The primary difficulty in the design of similar variable torque machines is in developing a satisfactory method of varying the machine constant at high RPM. Traditionally this has been accomplished by partial filling of the brake or by constricting the mass flow of the rotor in an otherwise full casing. The water dynamometer used the latter method. A recommended modification to the water brake would be to seal the junction between the rotating shaft and the casing with a Garlock seal. This would prevent water from leaking into the area of the bearings and would allow pressurization of the case and water ring to a greater extent. Reference 1 proposes a novel method of varying the machine constant in an energy absorber designed for aircraft carrier arresting gear. In this design, the fluid leaves the rotor in an axial direction and impinges on a stator mounted adjacent to the rotor. The stator absorbs the energy and directs the fluid axially back into the rotor. Torque variation is accomplished by changing the distance between the stator and the rotor. A 3 HP, 6" diameter test

model was used to verify this method of changing the machine constant, but the procedure has not been tested on a large machine and the flow phenomena occurring between the rotor and the stator when they are axially separated by an appreciable length have not been analyzed.

It can be concluded that a geometrically similar water brake of increased diameter would be capable of greater torque absorption. A dynamometer with an increased number of stages would also result in greater energy absorption, but a method of insuring that water was introduced to all the chambers and formed into a water ring would have to be devised.

A new proposal for varying the machine constant would be to mount a slotted flat plate on the inside of the stator with a mechanical linkage to the outside of the dynamometer. As the plate was rotated with respect to the stator, some of the radial grooves equally spaced around the stator face would be decreased in size or blocked completely by the flat plate. The plate could be cut in such a manner that the number of grooves in use would be gradually diminished, decreasing the machine constant and torque absorption. The primary difficulty with this proposal appears to be the possible leakage problem through the linkage.

More stable operation of the water brake would result if the water inlet supply could be made more constant by locating a water tank at a sufficient height to continually provide a constant head to the brake. If an open tank were located on the roof of the test cell and continually filled with water, sufficient head would be developed. Before a major test program is started using the water dynamometer, the water exit

pipe from the flow regulator should be connected to the compressor cooling water lines as an economy measure. A junction of reduced pressure would have to be selected to prevent a back pressure condition on the water dynamometer.

TABLE I

MACHINE CONSTANTS K_P CALCULATED WITH THREE DIFFERENT POWERS OF THE ROTOR DIAMETER-D

Run	$K_P \times 10^2$ Based on D^3	$K_P \times 10^3$ Based on D^4	$K_P \times 10^3$ Based on D^5	Pressure Ratio
Min required goal for 5.5"D	4.32	7.85	1.428	
6	3.66	6.66	1.210	1.18
7	3.95	7.19	1.307	1.17
8	4.08	7.43	1.350	1.51
9	4.15	7.54	1.371	1.52
10	.91	1.64	.300	1.11
11	2.68	4.88	.887	1.34
12	3.17	5.76	1.047	1.26
14	3.17	5.76	1.046	1.59
15	3.64	6.61	1.203	2.00
16	3.82	6.95	1.263	2.00
17	3.82	6.94	1.262	1.50
18	3.86	7.02	1.275	1.97
19	5.36	9.74	1.771	1.98
20	4.99 4.98 5.09	7.69 7.67 7.85	1.183 1.181 1.208	1.50 2.00 2.51
21	9.46 9.78	14.56 15.05	2.240 2.316	1.50 2.00
22	9.10 9.49	14.02 14.62	2.156 2.249	1.50 2.00
23	6.83 7.10	10.51 10.93	1.617 1.683	1.50 2.00

TABLE I (Continued)

Run	$K_P \times 10^2$ Based on D^3	$K_P \times 10^3$ Based on D^4	$K_P \times 10^3$ Based on D^5	Pressure Ratio
24	6.91 6.96	10.64 10.70	1.637 1.646	1.51 2.01
25	6.91 7.07	10.64 10.87	1.637 1.673	1.50 2.01
26	7.04	10.85	1.669	1.50
"Predicted K_P Run 26-27"	4.32	7.86	1.425	
27	5.892	9.070	1.397	1.50
28	4.352	6.695	.939	1.31

TABLE II

WATER DYNAMOMETER TEST RUNS - 1969

Run No.	Stator	Mod	Rotor	RPM (Usable Range)	Torque IN-lb (max)	HP (max)	$\frac{P_{to}}{P_2}$ (Turbine)	K_P and K_T x 10^3 Based on the Fifth Power of the Rotor Diameter	Remarks
1	none	-	1	12,000 dry 4000 wet	5	-	-		Bearing, operating check
2	none	-	1	0 - 4000	5	-	-		Brake with Drain
3	none	-	1	0 - 3000	5	-	-		Plexiglass face
4	1	Front Half	1	0 - 3000	7	-	-		½ Stator only
5	1	20° Offset	1	0 - 3680	10	-	-		Water fluctuations
6	1	20° Offset	1	2000-4000	100	6.3	1.18	1.210	Water recirculated
7	1	10° Offset	1	2000-10,000	220	28.2	1.48	1.307	±200 RPM>10,000 RPM dethrottle above 7500
8	1	Aligned	1	2000-10,000	279	37.2	1.60	1.350	Dethrottle above 7060
9	1	Aligned w/shim	1	1850-6000	255	24.3	1.52	1.371	No increase in Stability
10	2		1	5000-6000	53	4.9	1.11	.300	Very steady
11	3		1	5000 2000-6000	165	15.7	1.34	.887	Pipe failure at 6000 RPM

TABLE II (Continued)

Run No.	Stator	Mod	Rotor	RPM (Usable Range)	Torque IN-lb (max)	HP (max)	$\frac{P_{to}}{P_2}$ (Turbine)	K_P and K_γ x 10^3 Based on the Fifth Power of the Rotor Diameter	Remarks
12	4		1	2000-9950	376	59.3	1.95	1.047	Steady
13	4		1	2000-5000	145	11.5	1.28	1.123	Pipe disconnected at 5000 RPM
14	4		1	4000-13,000	410	69.5	2.01	1.046	Steady to 12,000 RPM
15	5	Shim in place	1	1970-10,000	422	70.0	2.00	1.203	Unsteady above 10,000 RPM
16	5	No shim	1	3000-13,000	442	69.3	2.01	1.263	Axial clearance .010. Air used
17	5		1	4000-10,000	249	30.0	1.51	1.262	Unsteady above 10,000 RPM
18	5		1	4050-17,700	625	116.5	2.51	1.275	Unsteady above 14,000 RPM
19	6		1	2930-10,800	640	99.5	2.51	1.771	First angled grooves run
20	7	No Mid-Stator	2	3000-4360 -5800 -6840	268 473 673	18.5 43.5 73.0	1.50 2.00 2.51	1.183 1.181 1.208	Very unsteady upon dethrottling
21	8	Slotted Mid-Stator	2	3000-8800 4300-11,300	287 510	29.5 66.7	1.50 2.00	2.240 2.316	Slightly unsteady air helped
22	8	Slotted Mid-Stator	2	3320 4360	283 509	14.9 35.2	1.50 2.00	2.156 2.249	Unsteady dethrottle
23	9	Uncut Mid-Stator	2	3000-7000 4970	281 495	26.1 39.0	1.50 2.00	1.617 1.683	Unsteady dethrottle

TABLE II (Continued)

Run No.	Stator	Mod	Rotor	RPM (Usable Range)	Torque IN-lb (max)	HP (max)	$\frac{P_{to}}{P_2}$ (Turbine)	K_{p_3} and K_f x 10^3 Based on the Fifth Power of the Rotor Diameter	Remarks
24	7	Spacer Left Out	3	3000-5060	502	40.3	2.00	1.637 1.646	Water supply fluctuations
25	7	Stator Spacer	3	2000-5060	510	40.9	2.00	1.637 1.673	Stator spacer installed
26	7	65" D Rotor	1	3010-4990	510	40.4	2.00	1.669	Rotors together
27	7	Back Stator as in Runs 19-20	1	3000-5450	493	42.6	2.00	1.397	6.5" D Rotor
28	3	Optimum	1	3000-9440	271	30.3	1.50	.939	6.5" D Rotor

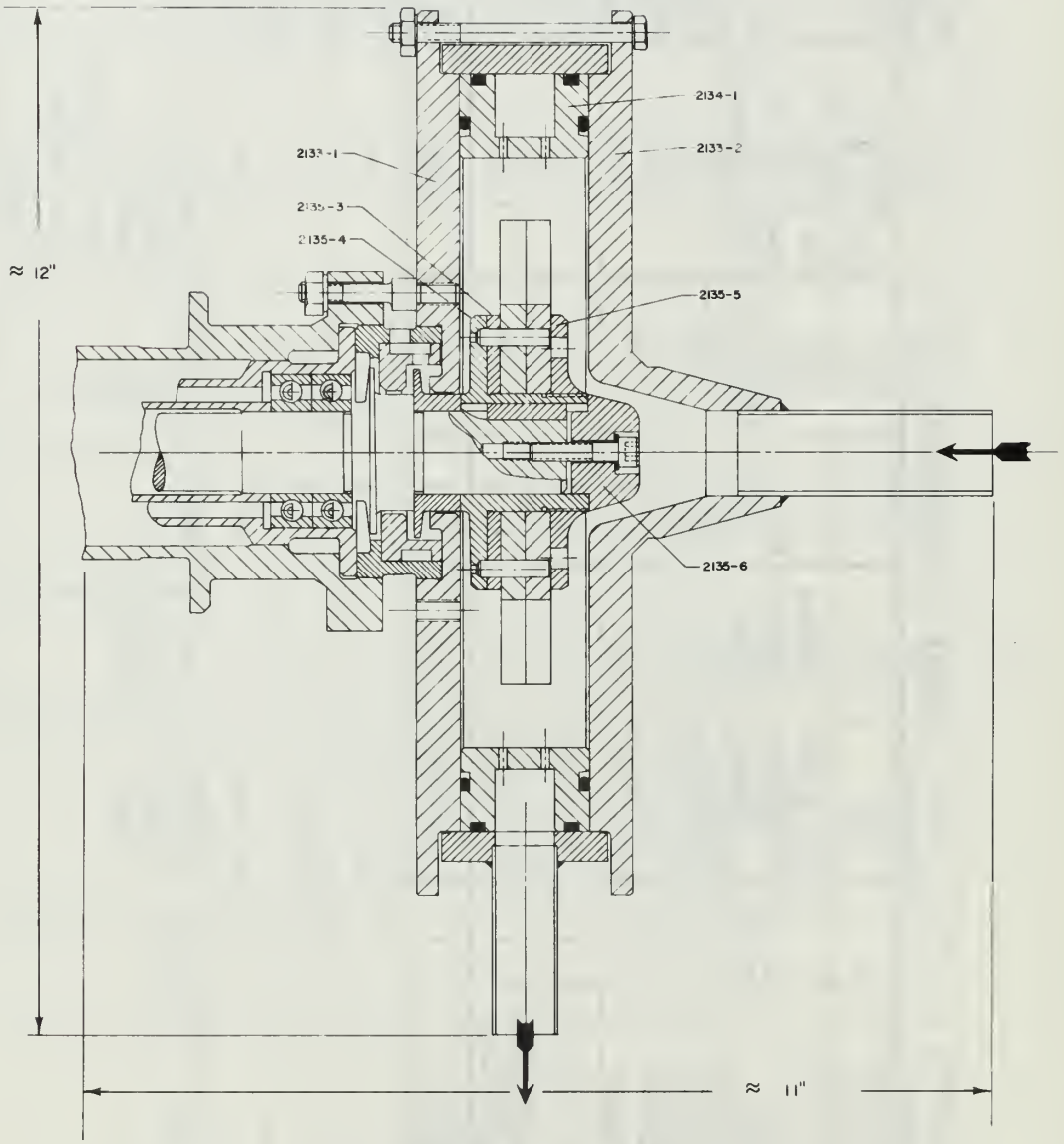

Figure 1. Internal Details of the Water Dynamometer

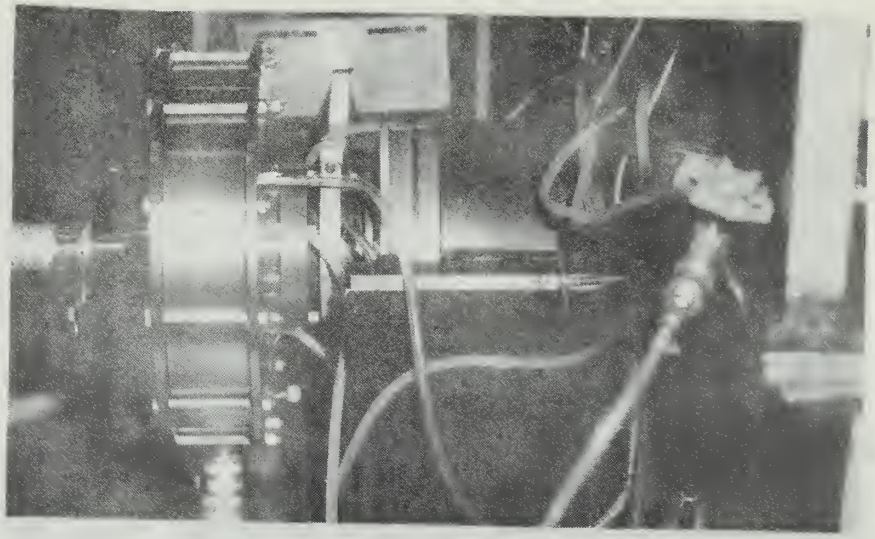

Figure 2. Side View of the Dynamometer Showing Mounting Details, Air Taps, and the Dynamometer Bearing Stand

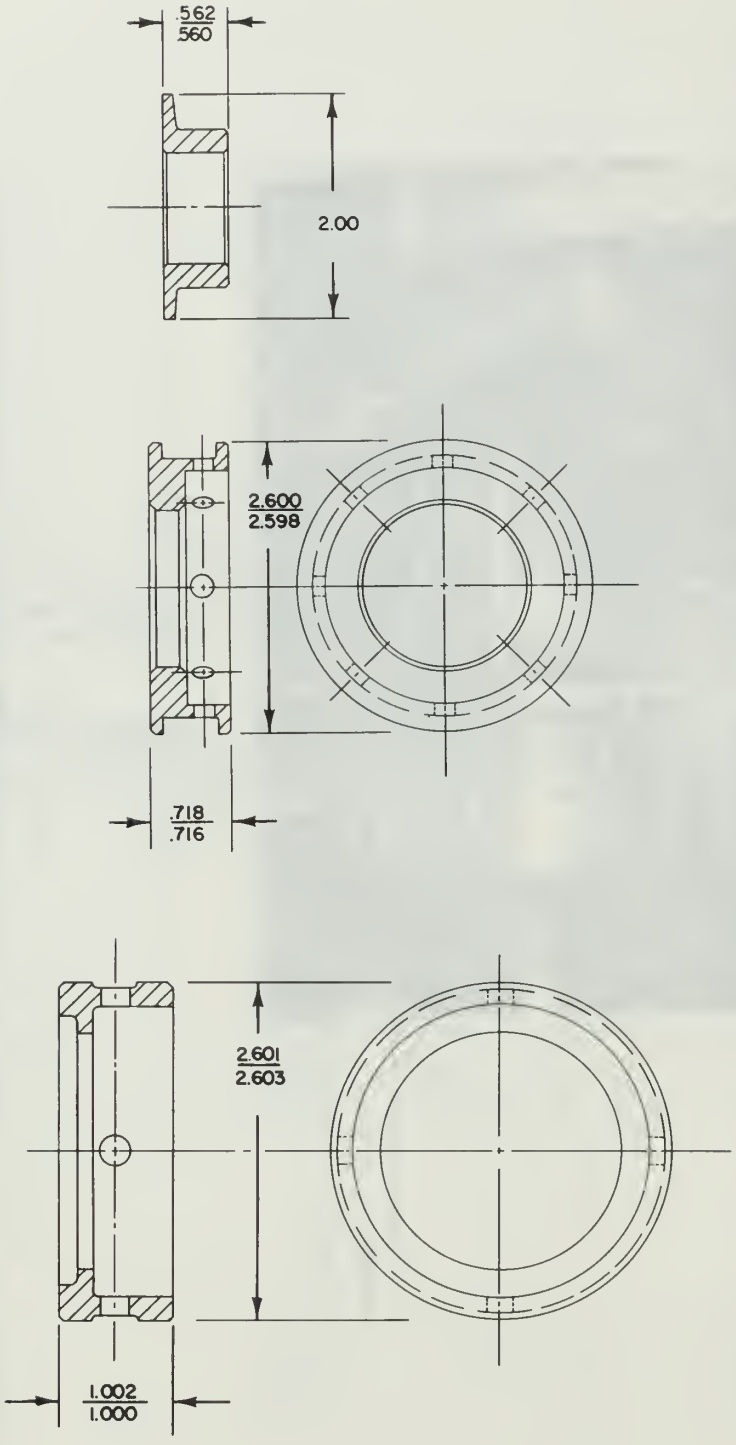

Figure 3. Mounting Adapters for the Water Dynamometer

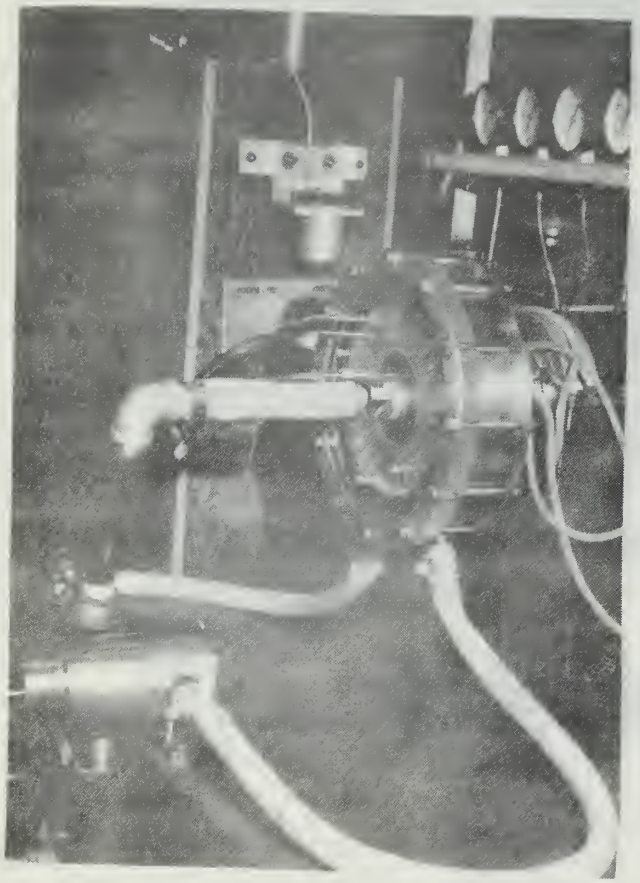

Figure 4. Overview of the Dynamometer Installation

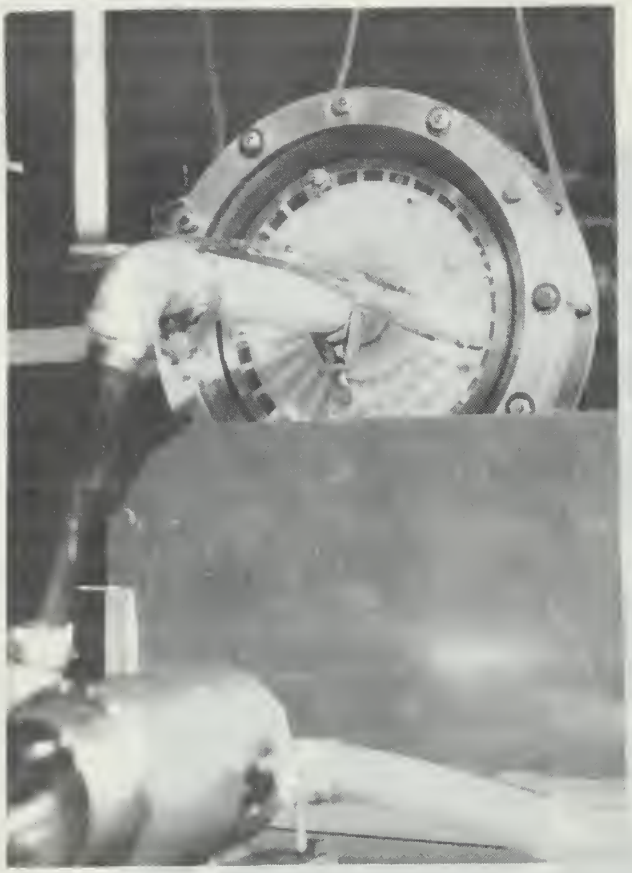

Figure 5. The Dynamometer in Operation Utilizing a Plexiglass Front Face. A Water Leakage Collector is in the Foreground.

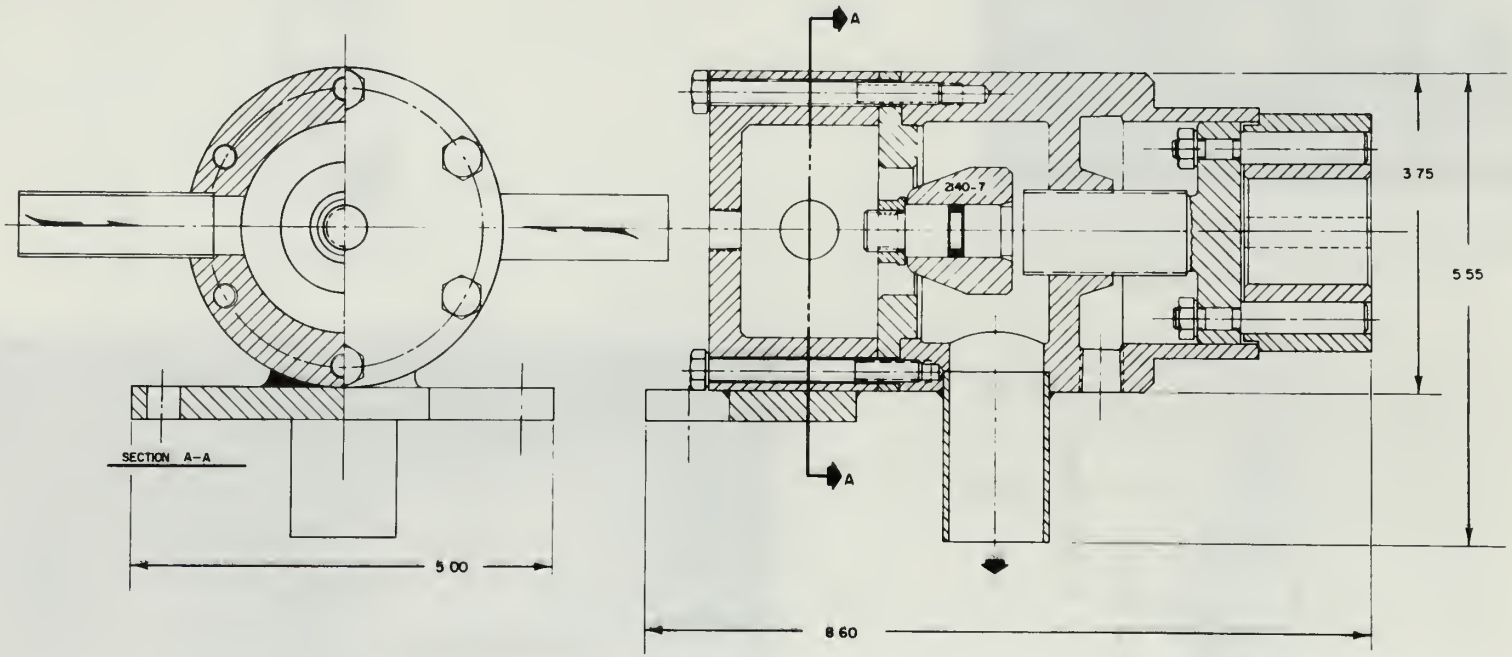

Figure 6. Internal Details of the Water Regulating Valve

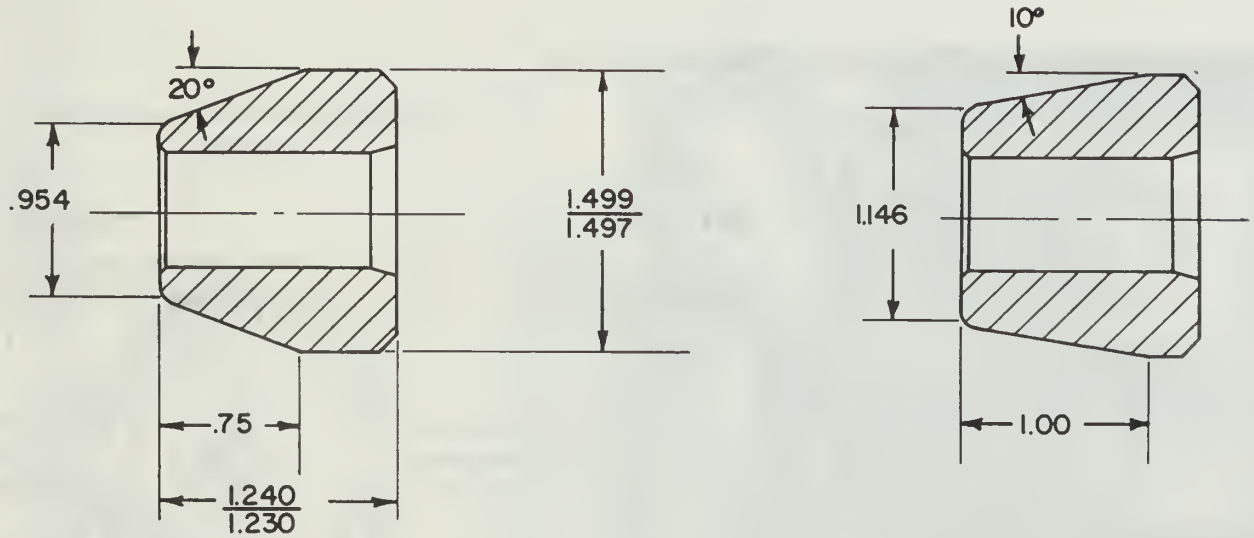

Figure 7. The Water Regulating Valve (Part 2140-7) Showing the Redesign to an Angle of 10 degrees

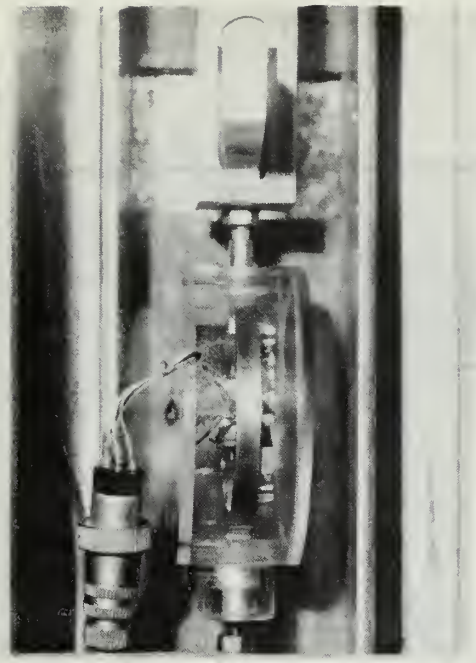

Figure 8. The Dynamometer Force Capsule

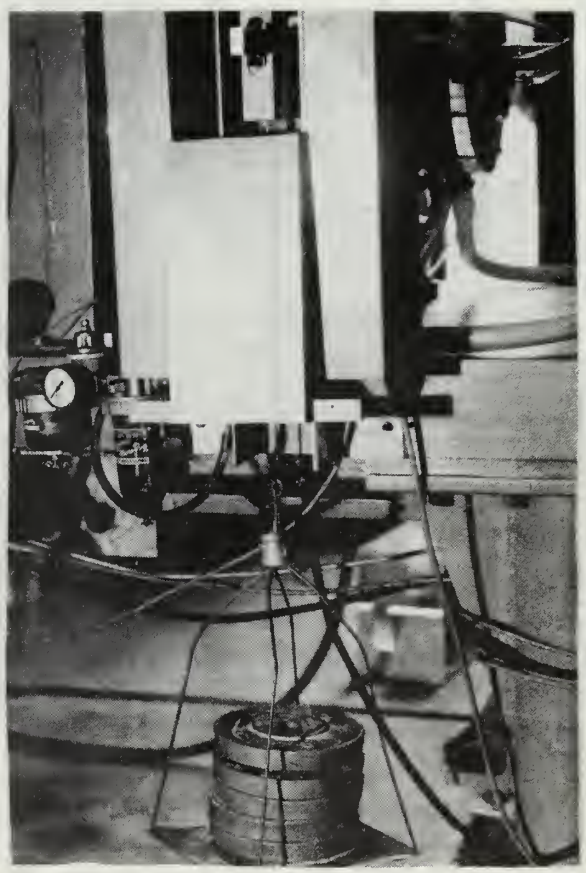

Figure 9. The Force Capsule Calibration Procedure, Water Brake in Background

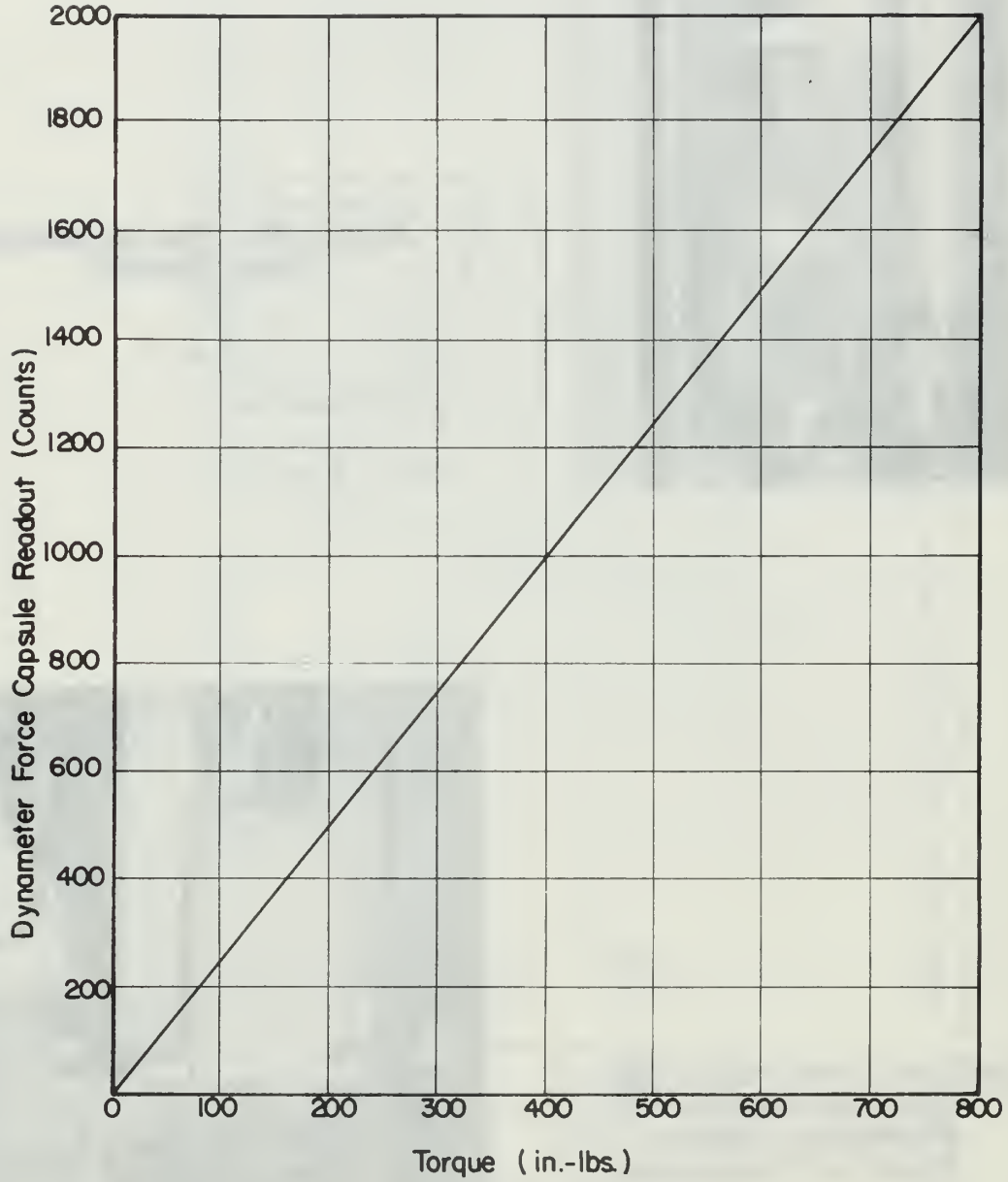

FIGURE 10. DYNAMOMETER TORQUE CALIBRATION CURVE

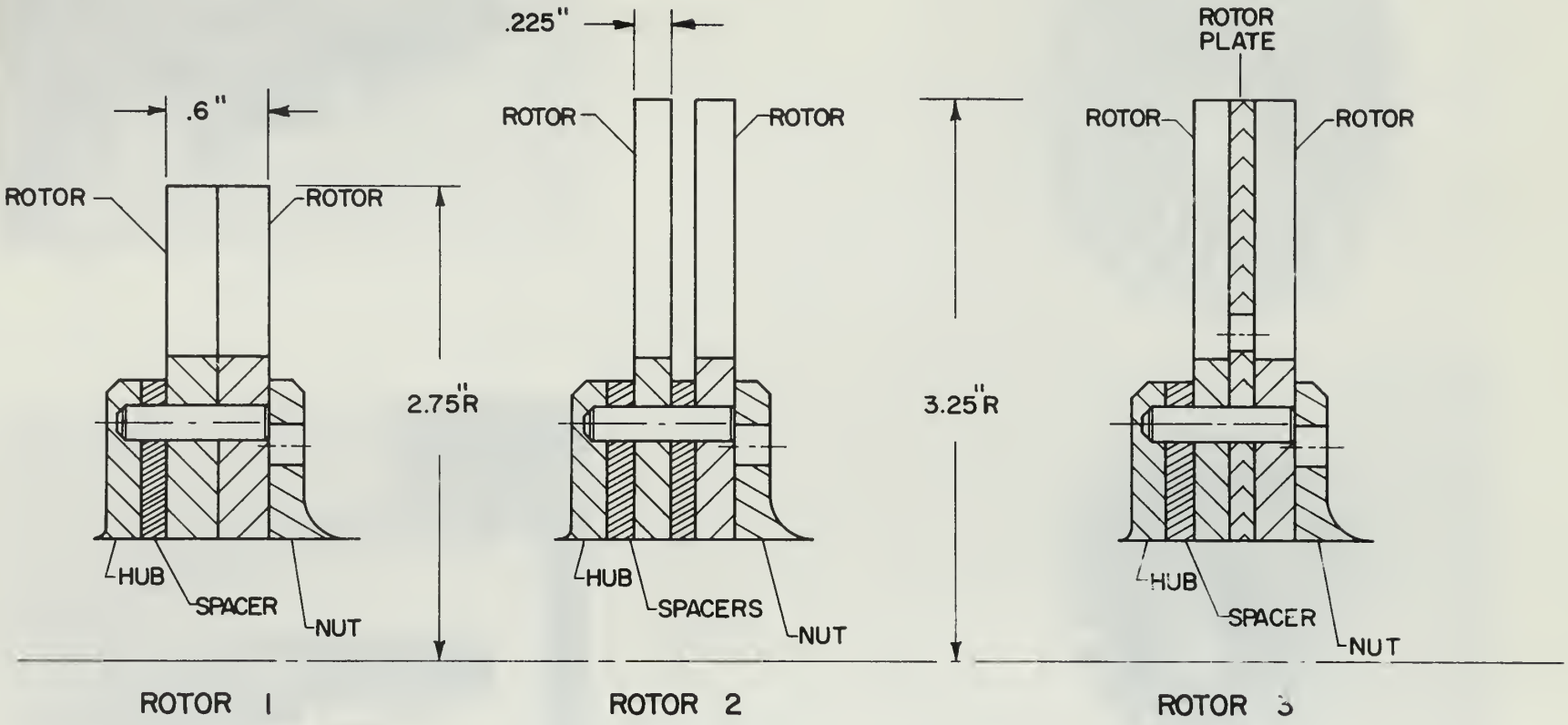

FIGURE 11. WATER BRAKE ROTOR CONFIGURATIONS.

Figure 12. Rotor Configuration One

Figure 13. Rotor Configuration Three

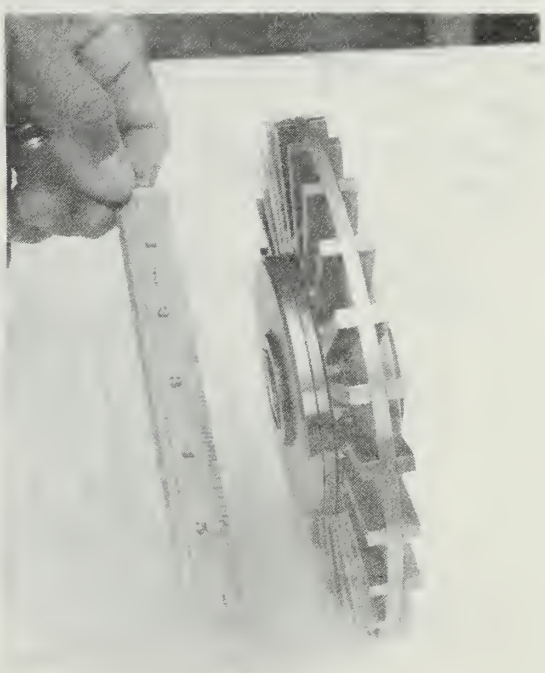

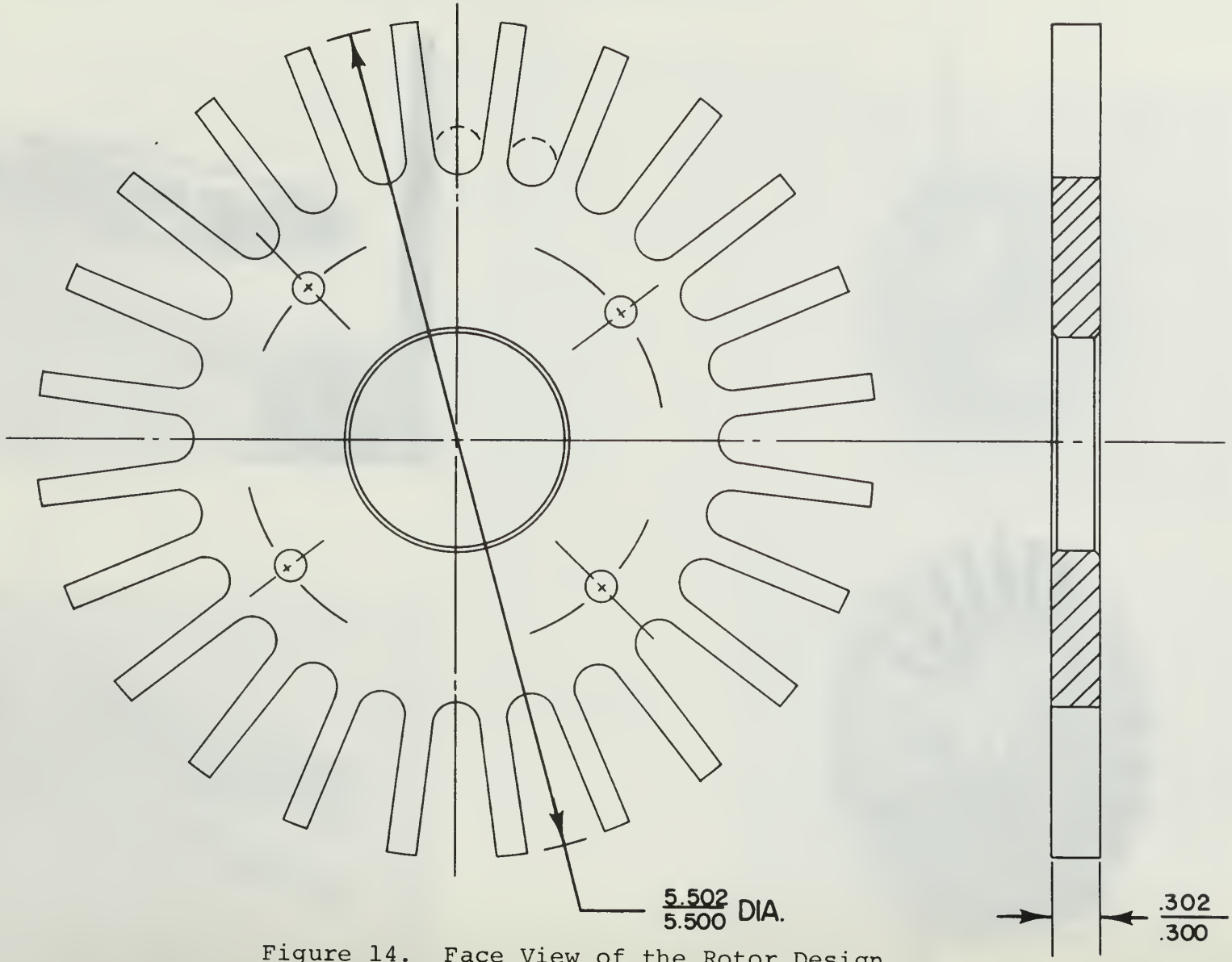

Figure 14. Face View of the Rotor Design

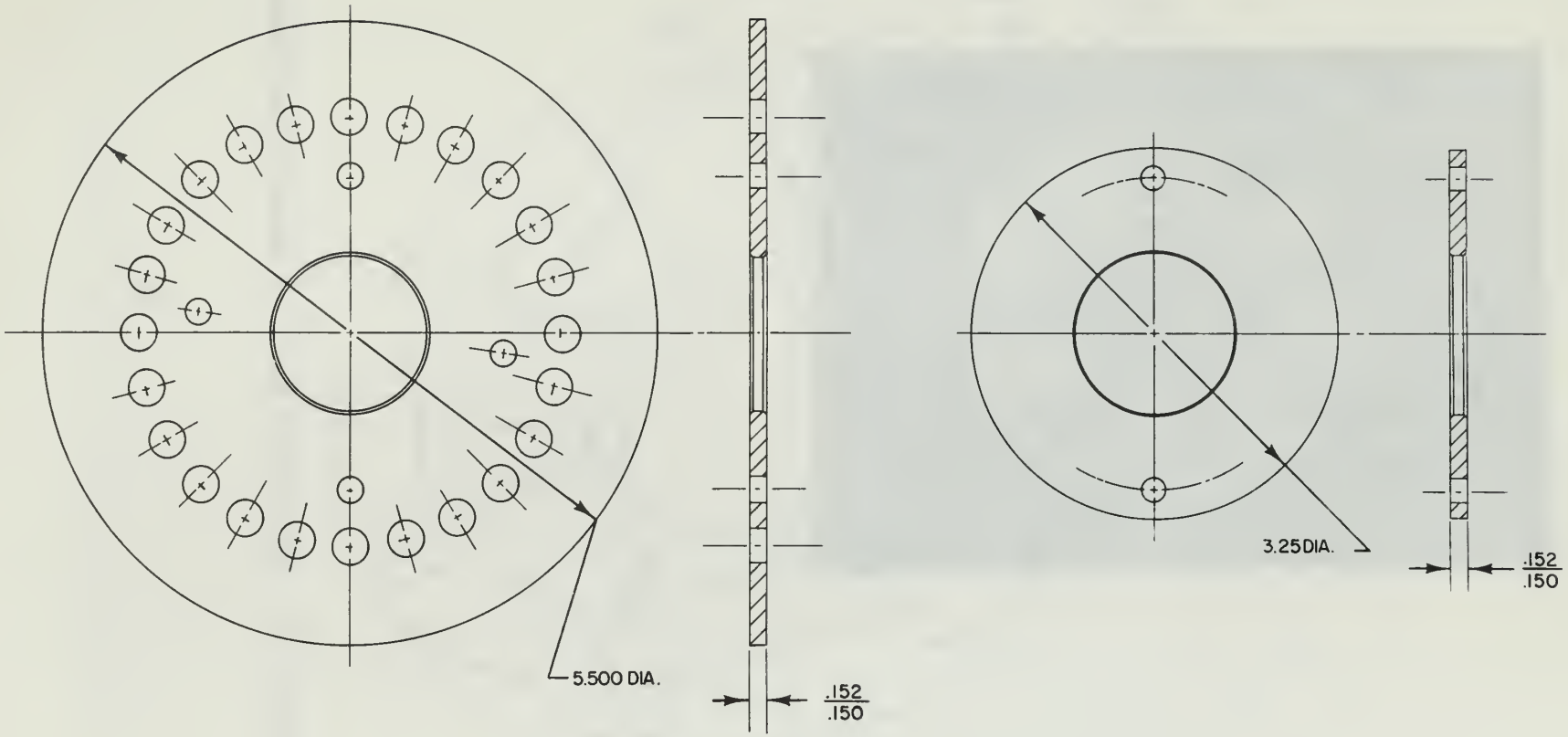

Figure 15. The Rotor Plate and Rotor Spacer Design

Figure 16. The Front Half of Stator Configuration One

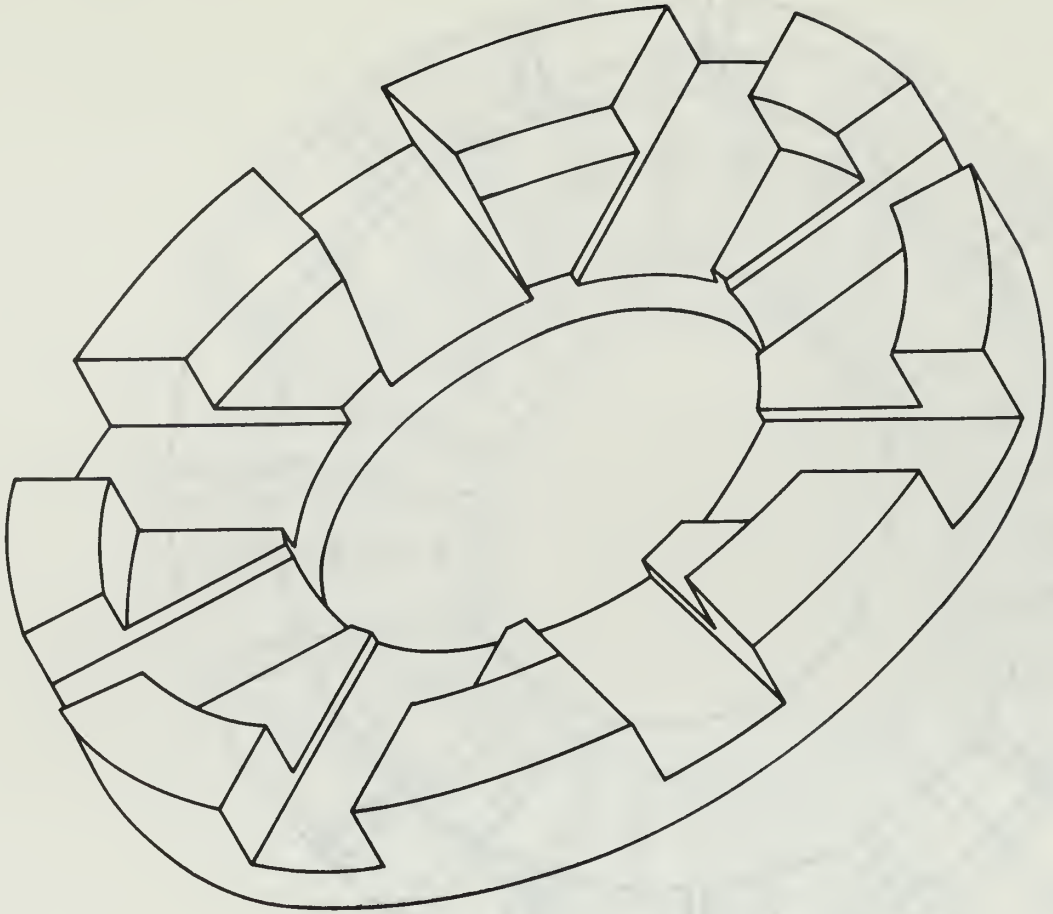

Figure 17. Stator Configuration One

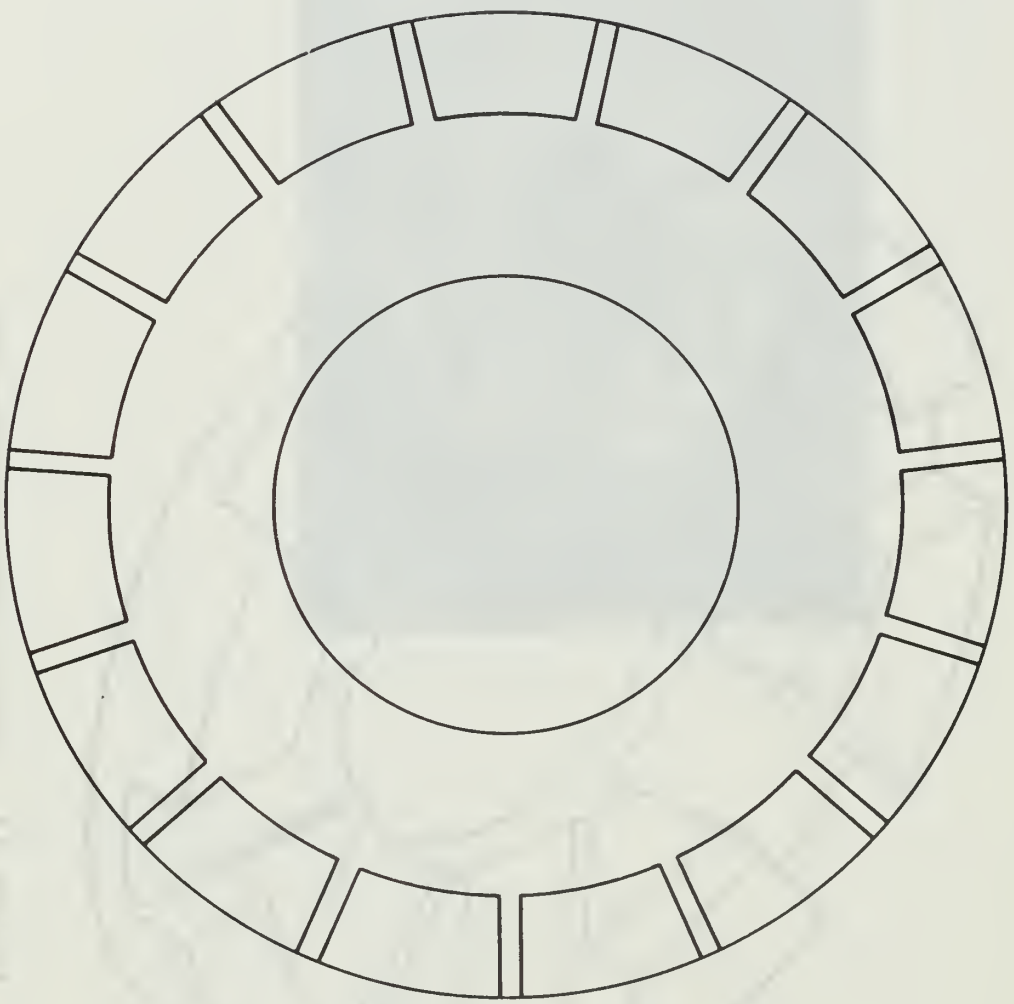

Figure 18. Stator Configuration Two

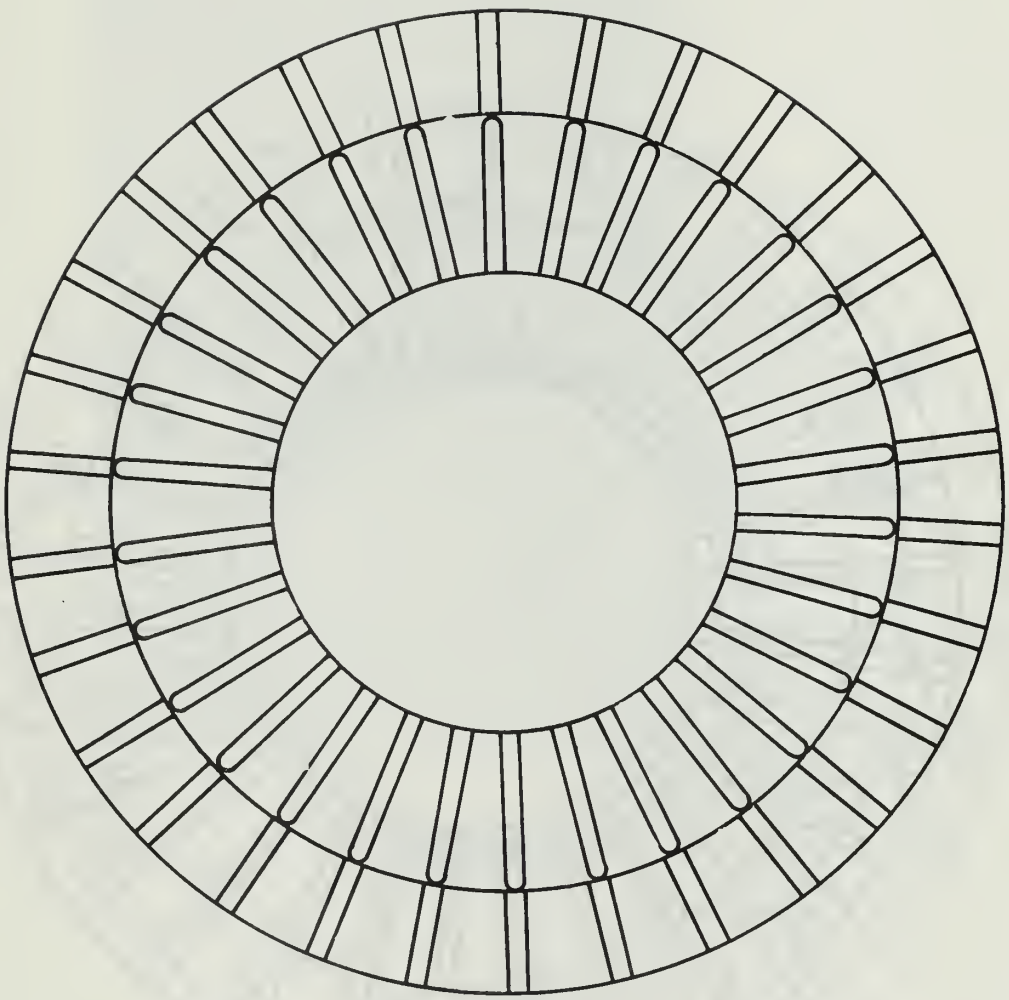

Figure 19. Stator Configuration Three

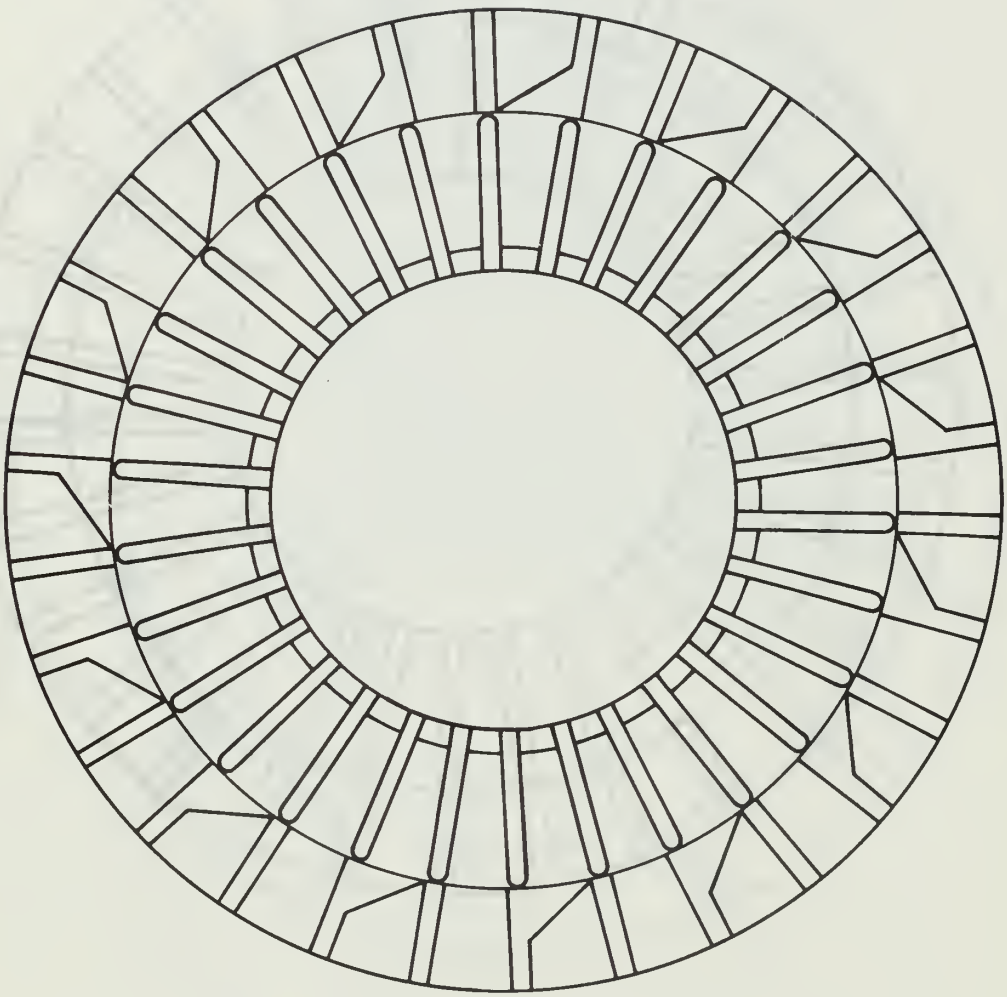

Figure 20. Stator Configuration Four

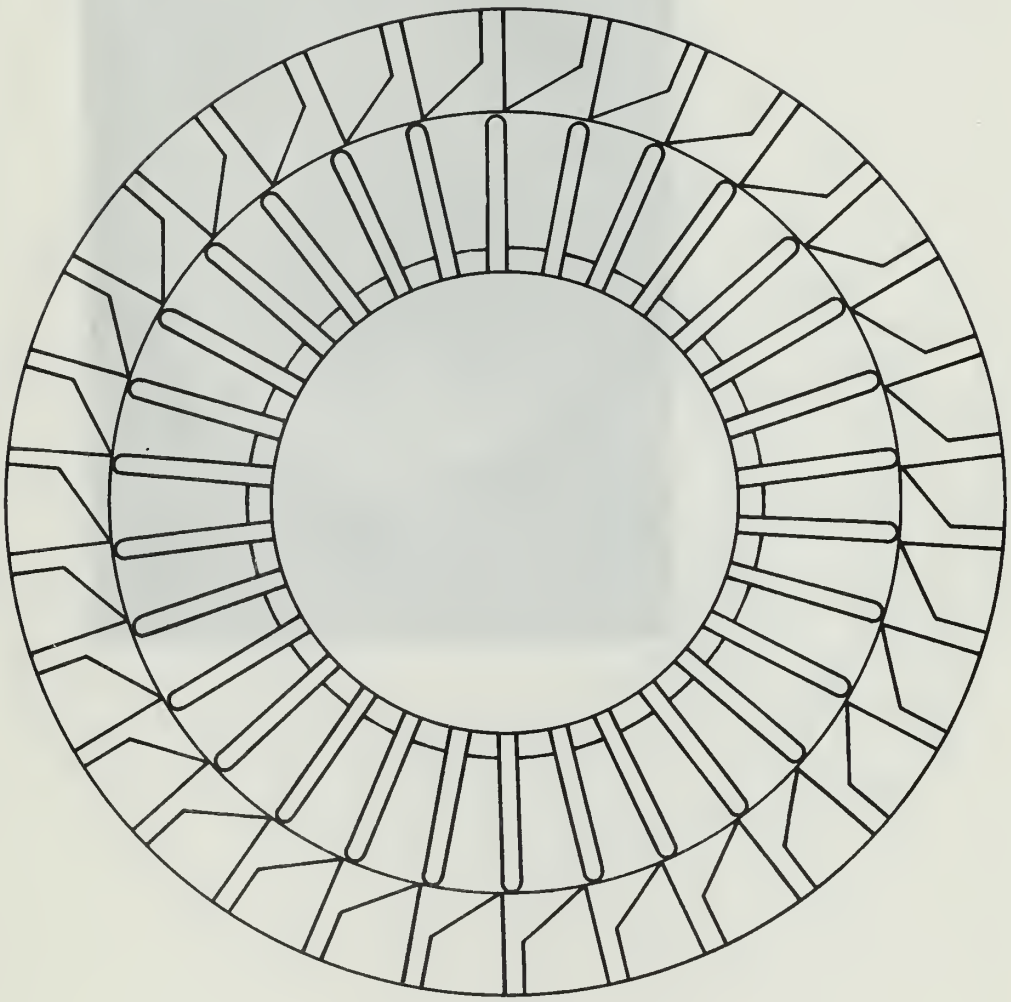

Figure 21. Stator Configuration Five

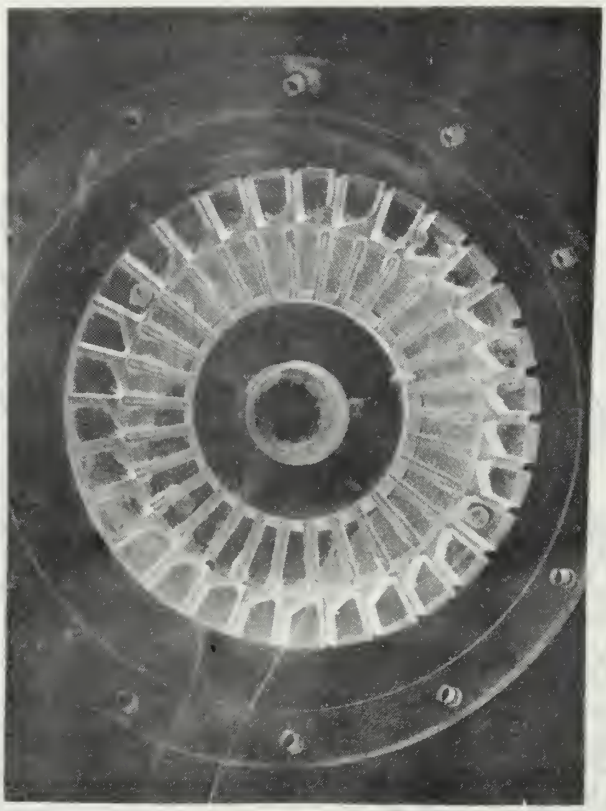

Figure 22. Stator Configuration Five Mounted on the Plexiglass Front Face, Showing Evidence of Cavitation and Turbulence Damage

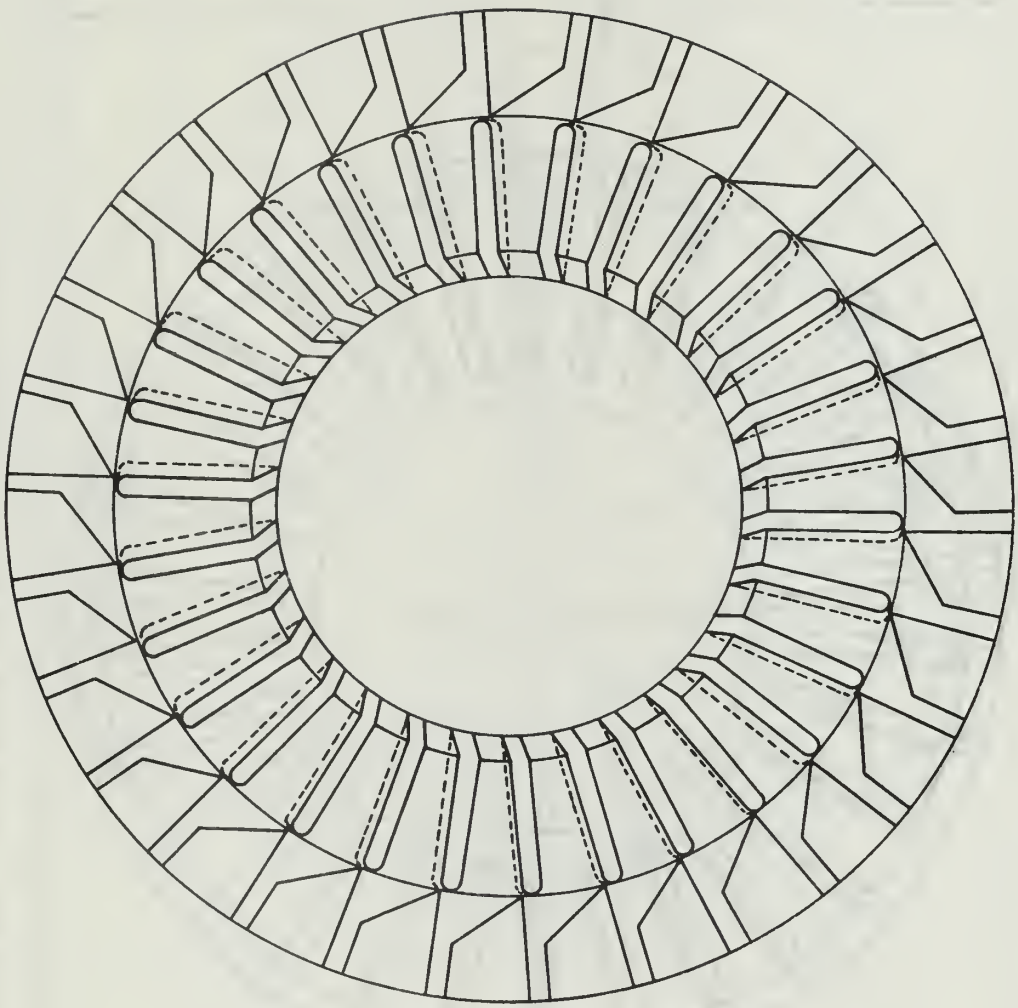

Figure 23. Stator Configuration Six

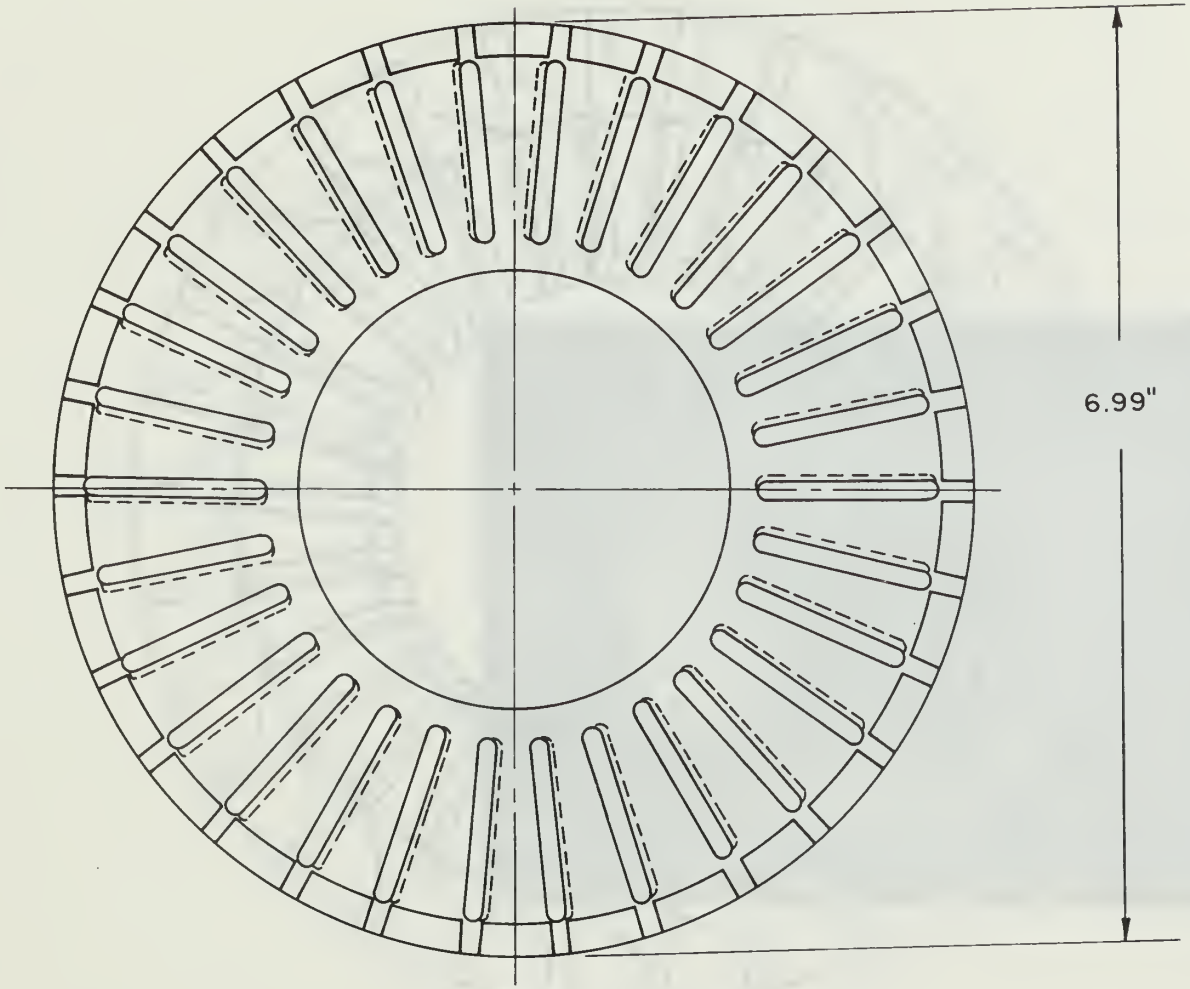

Figure 24. Back Half of Stator Configuration Seven

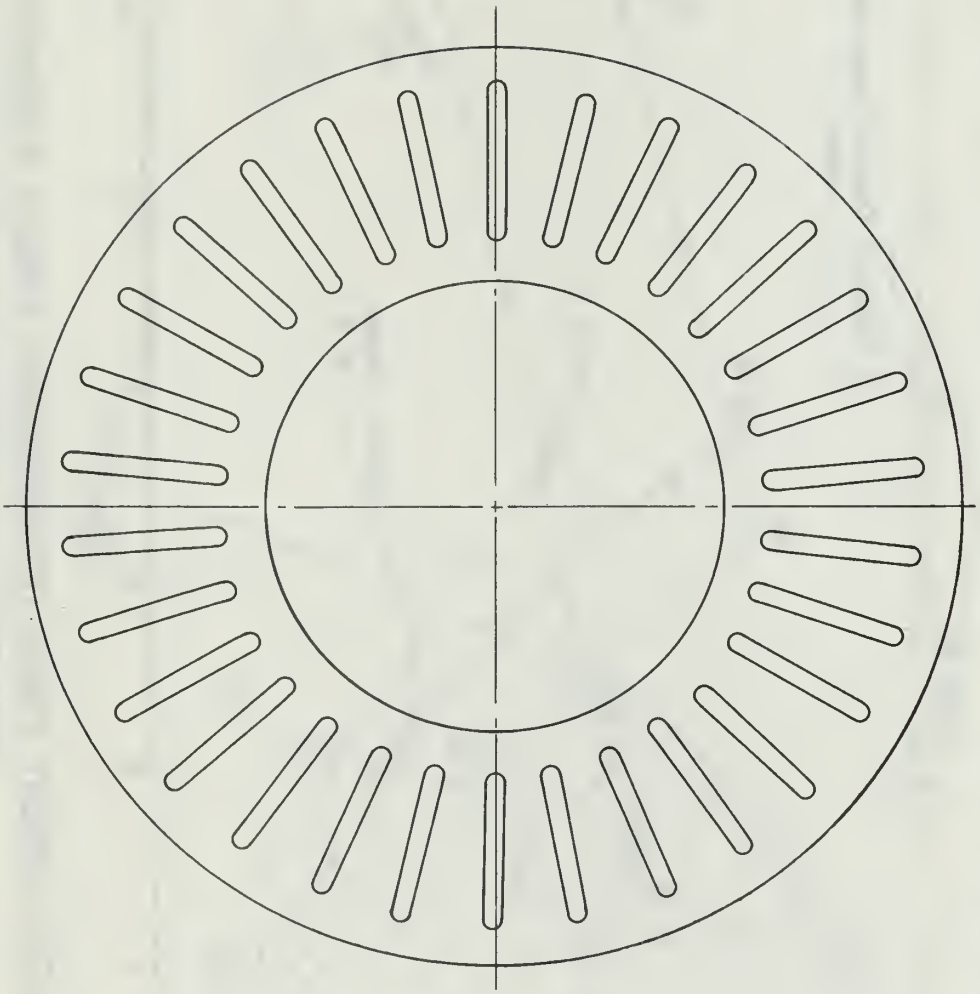

Figure 25. Slotted Stator that was Located Between the Two Rotors for Stator Configuration Eight

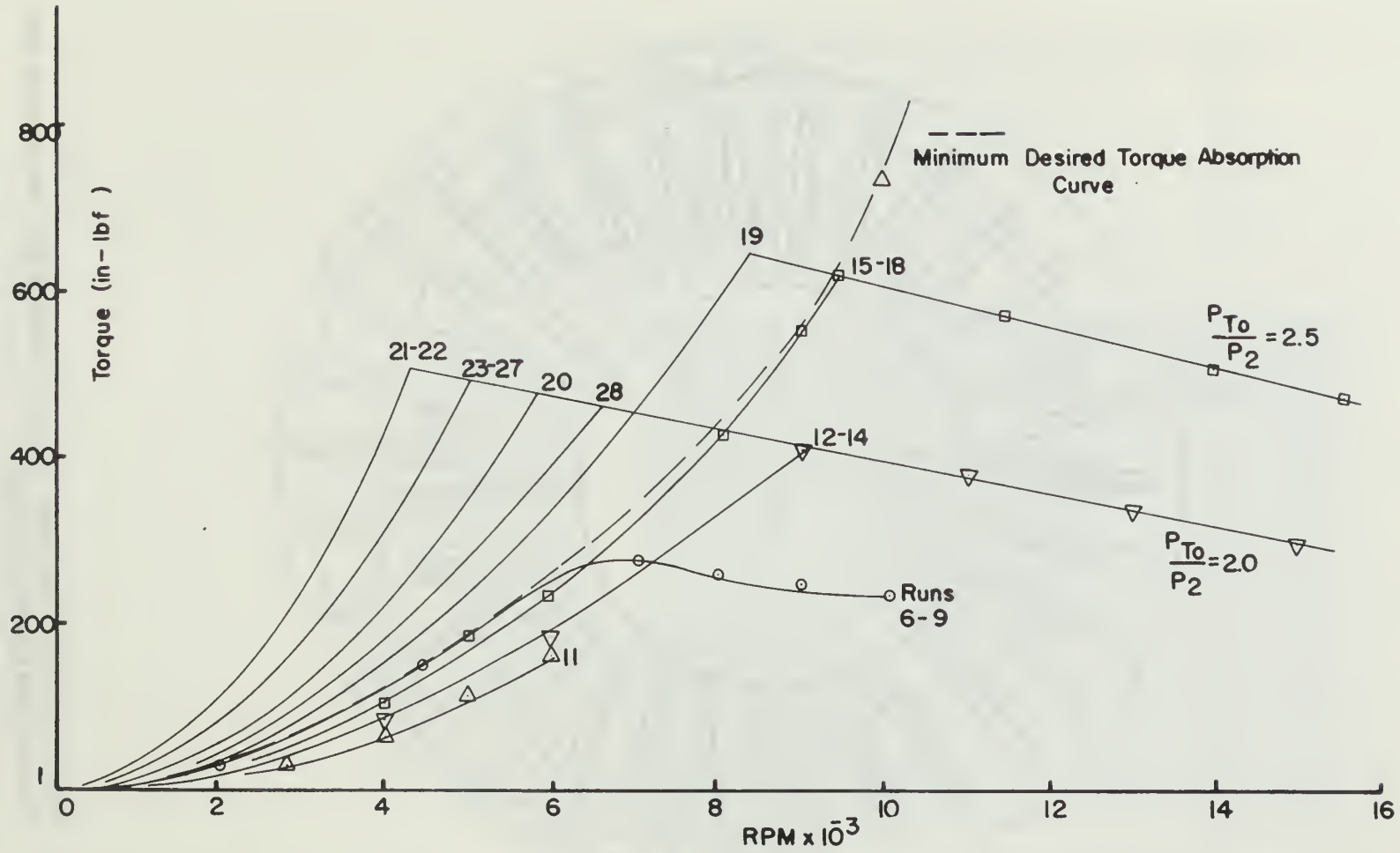

FIGURE 26. THE DEVELOPMENT PHASE. DYNAMOMETER TORQUE ABSORPTION VS. RPM FOR THE VARIOUS RUNS.

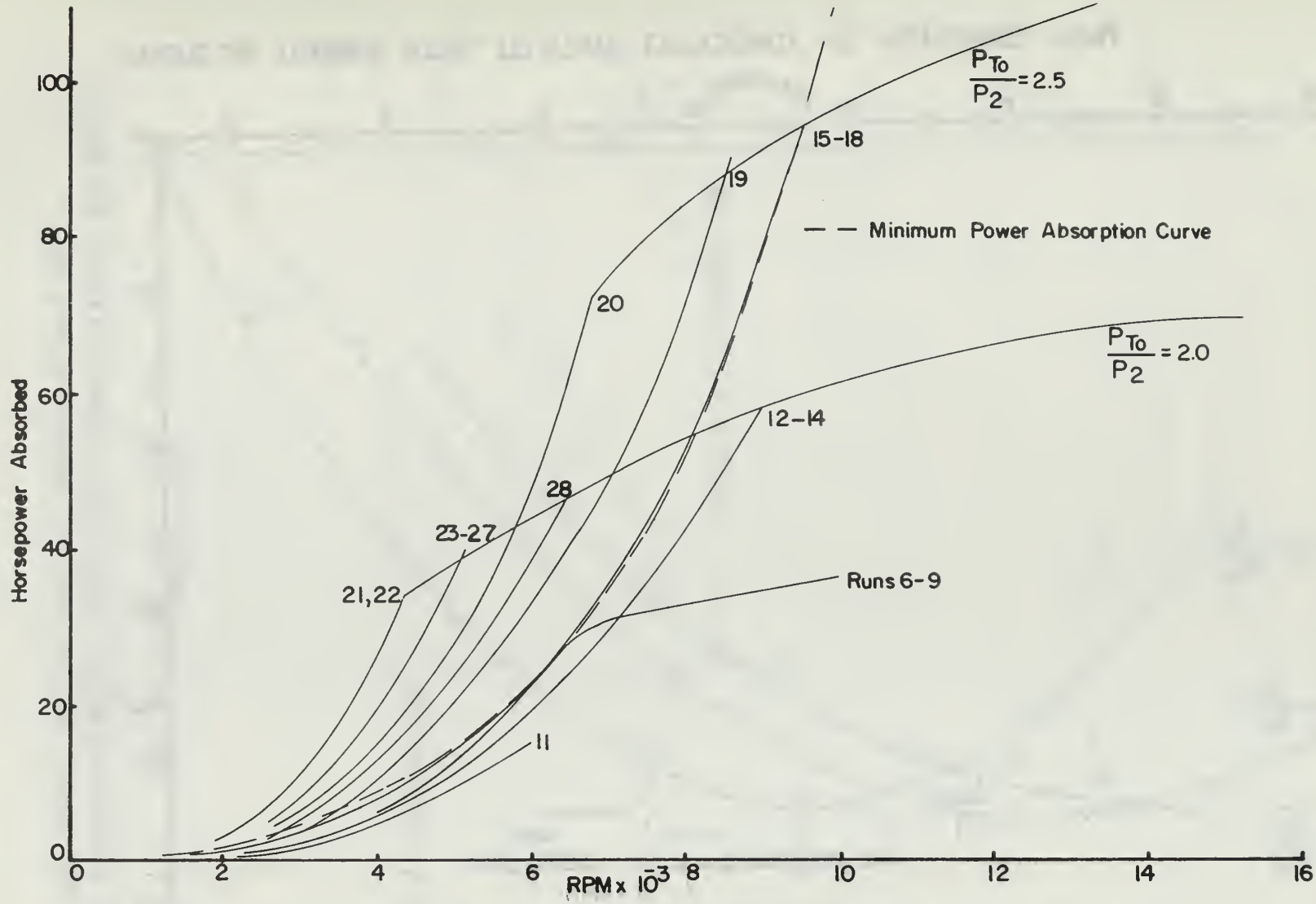

FIGURE 27. THE DEVELOPMENT PHASE. HORSEPOWER ABSORBED VS. RPM

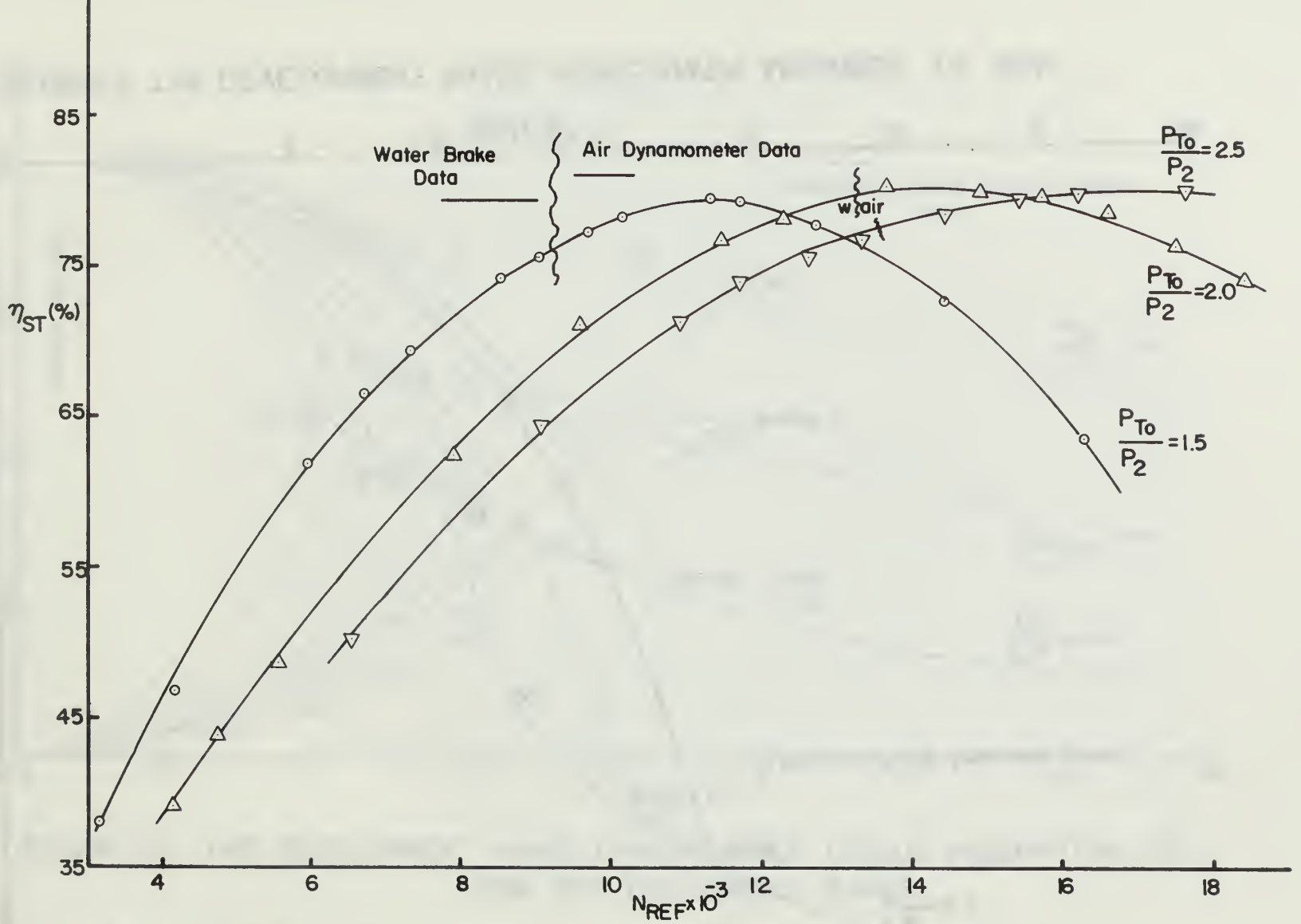

FIGURE 28. TURBINE TOTAL TO STATIC EFFICIENCY VS. REFERRED RPM

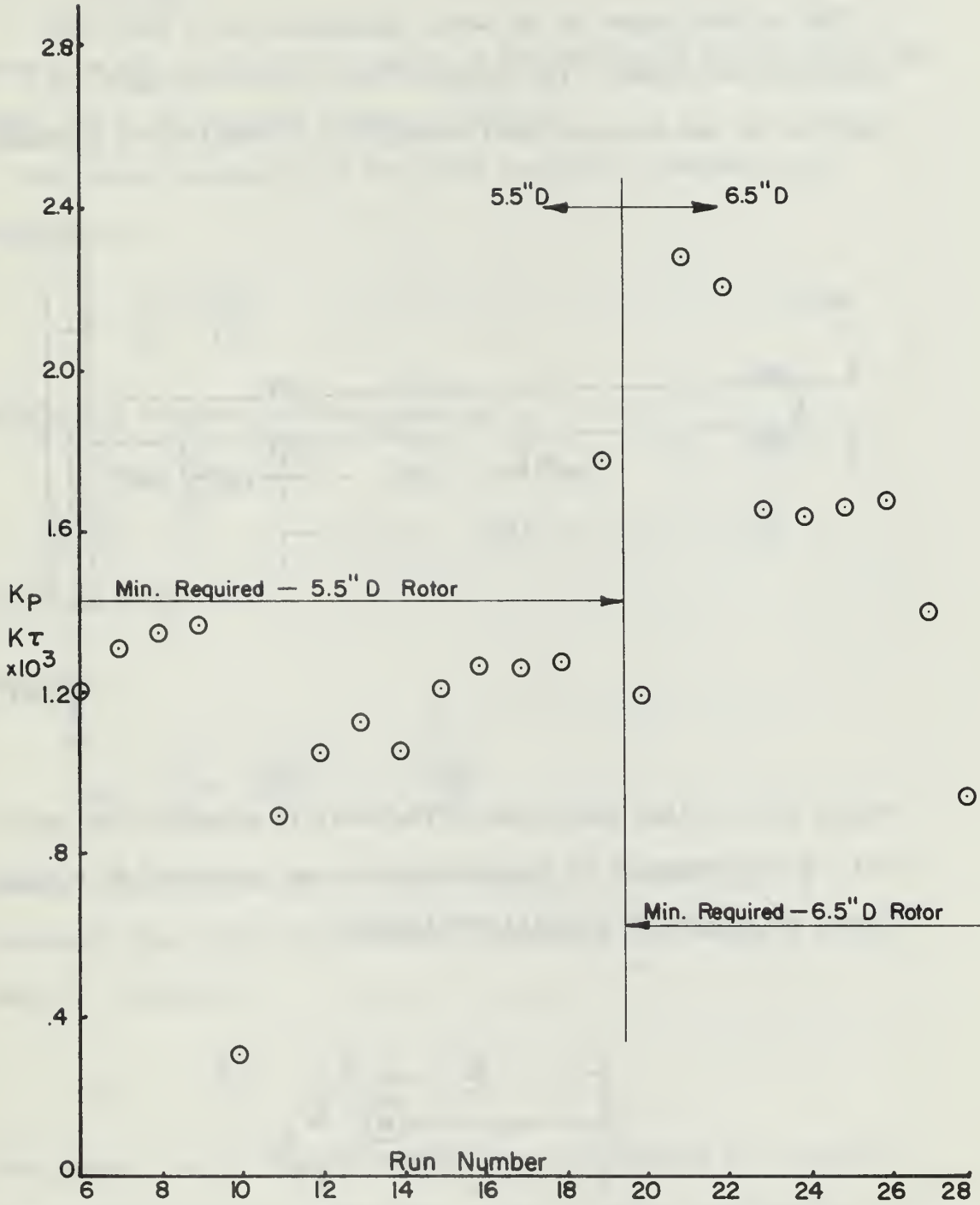

FIGURE 29. TORQUE-POWER COEFFICIENT VS. RUN NUMBER BASED ON FIFTH POWER OF THE ROTOR DIAMETER.

APPENDIX A

CRITICAL SPEED OF THE ROTOR SHAFT

The critical speed of the water dynamometer rotor shaft was calculated as follows: The stainless steel rotor and shaft are supported by two precision ball bearings in a cantilevered arrangement.

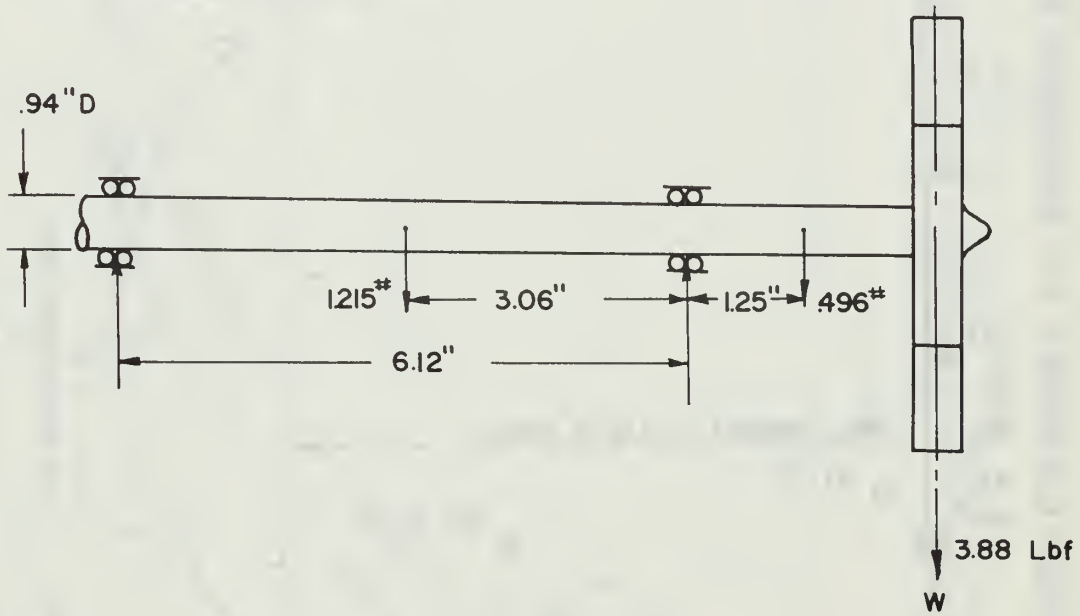

Shigley [Ref. 7] has found that if the shaft is assumed to be weightless, an approximation of the system above can be reduced to a weight mounted on the end of a cantilever spring.

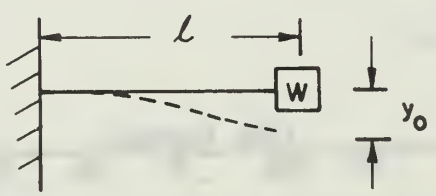

The static deflection of the spring is

$$y_o = \frac{W\ell^3}{3EI}$$

where ℓ is the length of the spring, E the modulus of elasticity of the shaft, and I the flexural moment of inertia.

The spring constant k is the force required to produce unit deflection, or

$$k = \frac{W}{y_o} = \frac{3EI}{\ell^3}$$

The natural frequency of the system is

$$\omega_n = \sqrt{\frac{k}{m}}$$

with $m = \frac{W}{g}$

there is,

$$\omega_n = \sqrt{\frac{k}{m}} = \sqrt{\frac{3EI/\ell^3}{W/g}} = \sqrt{\frac{3EIg}{W\ell^3}}$$

However, for a system with a single degree of freedom, $y_o = \frac{W}{k}$ represents the static deflection of the spring with weight W acting upon it. Therefore

$$\omega_n = \sqrt{\frac{k}{m}} = \sqrt{\frac{g}{W/k}} = \sqrt{\frac{g}{y_o}}$$

This gives a useful simplified expression for finding the natural frequency of the system. The same equation can be developed for a system where the shaft is not assumed to be weightless if the static deflection can be found.

For a shaft that is supported at both ends and which rotates at an angular velocity ω, the above-listed formula can be obtained also by balancing the centrifugal force due to the shaft deflection with the weight of the shaft.

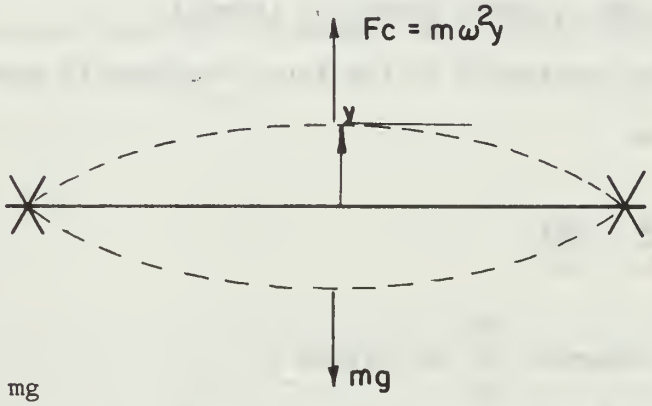

$$m\omega^2 y = mg$$

$$\omega = k\sqrt{\frac{g}{y}}$$

where y is the deflection of the shaft due to the force of gravity mg. For the water dynamometer rotor

$$\rho_{\text{STAINLESS STEEL}} = 0.286 \frac{\text{lbf}}{\text{IN}^3}$$

$$E = 28.5 \times 10^6 \frac{\text{lbf}}{\text{IN}^2}$$

$$I_{\text{ROUND SHAFT}} = \frac{\pi D^4}{64} = 0.0491\ D^4$$

The weights of the shaft segments are found from

$$W = \rho V$$

where V is the volume of the shaft segments.

These weights, the rotor weight, and the dimensions of the rotor system are indicated on the drawing at the beginning of this Appendix. The deflections caused by the three weights can be added algebraically to yield

$$y_o = \Sigma \frac{W\ell^3}{3EI} = 0.813 \times 10^{-5} \text{ IN}$$

$$\omega_n = \sqrt{\frac{g}{y_o}} = \sqrt{\frac{386 \text{ in/sec}^2}{0.813 \times 10^{-5} \text{IN}}} = 6.9 \times 10^3 \frac{\text{radians}}{\text{sec}}$$

Hence,

$$N_{CRIT} = 65{,}800 \text{ RPM.}$$

Thus the critical speed of the rotor shaft is far above the operating range of the turbine-water brake combination.

APPENDIX B

STRESS CALCULATIONS OF THE WATER DYNAMOMETER COMPONENTS

A. THE ROTOR STRESSES

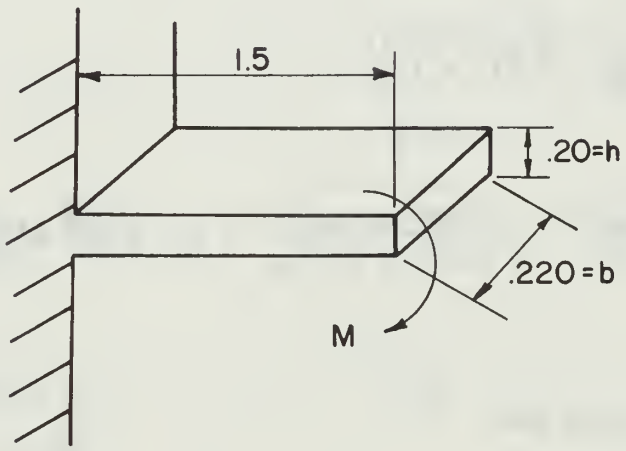

For the rotors of 6.50" diameter that have 48 blades with the dimensions shown above, the bending stress at 700 IN-lbf torque absorption is calculated from

$$M = \frac{700}{48} \text{ IN-lbf} = 14.58 \simeq 15 \text{ IN-lbf per blade}$$

$$I = \frac{1}{12} bh^3 = \frac{(.22)\ (.2^3)}{12} = 1.47 \times 10^{-4} \text{ IN}^4$$

$$\sigma_B = \frac{My}{I} = \frac{(15 \text{ IN-lbf})\ (.1 \text{ IN})}{1.47 \times 10^{-4} \text{ IN}^4} = 10{,}204 \frac{\text{lbf}}{\text{IN}^2}$$

The stresses caused by centrifugal force at

$$N = 20{,}000 \text{ RPM, or, } \omega^2 = 4.386 \times 10^6 \frac{\text{radians}^2}{\text{sec}^2}$$

are obtained as follows:

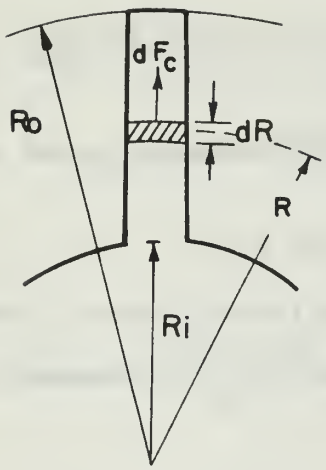

$dF_c = A \rho \omega^2 R \, dR$

$R_o = 3.25"$

$R_i = 1.75"$

A = cross sectional area of blades

Stainless steel with a specific weight of 0.286 lbf/IN^3 has a mass density ρ of

$$\rho = \frac{(.286)\ lbf/IN^3}{(32.17 \frac{lbf}{lbm} \frac{ft}{sec^2})(\frac{12\ IN}{ft})} = 7.41 \times 10^{-4} \frac{lbm\ sec^2}{IN^4}$$

Integrating the centrifugal force dF_c acting or the volume element between R and R + dR, gives

$$F_c = \rho\omega^2 A\left[\frac{R_o^2 - R_i^2}{2}\right] = \rho\omega^2 A\left[\frac{R_o + R_i}{2}\right]\left[R_o - R_i\right]$$

$$\sigma_c = \frac{F_c}{A} = \rho\omega^2\left[\frac{R_o + R_i}{2}\right]\left[R_o - R_i\right]$$

$$\sigma_c = (7.41 \times 10^{-4})(4.386 \times 10^6)(2.50)(1.50) = 12{,}187 \frac{lb}{IN^2}$$

$$\sigma_{yield} = 35{,}000 \frac{lb}{IN^2} \quad \text{(Stainless 301 Annealed)}$$

With a safety factor of 25%, the combined stresses should not exceed

$$yield = (.75)(35{,}000) = 26{,}250 \frac{lb}{IN^2}$$

The combined stresses are:

$$\sigma_{yield} = \sigma_B + \sigma_c = 10,204 + 12,187 = 22,391 \frac{lb}{IN^2}$$

Therefore, the rotor stresses for this configuration are acceptable.

B. THE STRESSES IN THE FLAT PLEXIGLASS PLATE

The axial force on the front face is the product of pressure times the differential area. From Paragraph IV-D the pressure P at a radius R is

$$P = \frac{\rho \omega^2}{2} [R^2 - R_i^2]$$

if P = 0 at R = R_i. The axial force dF_A acting on the area $dA = 2\pi RdR$ is

$$dF_A = PdA = \pi \rho \omega^2 [R^3 dR - R_i^2 RdR]$$

The total axial force F_A between R_i and R_o is

$$F_A = \int_{R_i}^{R_o} dF_A = \pi \rho \omega^2 \left[\frac{R_o^4 - R_i^4}{4} - R_i^2 \left(\frac{R_o^2 - R_i^2}{2} \right) \right]$$

or

$$F_A = \frac{\pi \rho \omega^2}{2} \left[\frac{R_o^4}{2} - R_i^2 \left(R_o^2 - \frac{R_i^2}{2} \right) \right]$$

For

$$R_o = 3.25", \quad R_i = 1.75"$$

$$F_A = \frac{\pi \rho \omega^2}{2} \boxed{28.125}$$

For N = 20,000 RPM, or, $\omega_{rotor} = 2094 \frac{\text{radians}}{\text{sec}}$

The water ring rotates at approximately

$$\tfrac{1}{2}\omega_{rotor} = 1047 \frac{\text{radians}}{\text{sec}}$$

Hence,

$$\omega^2_{water} = \frac{1.096 \times 10^6}{\text{sec}^2}$$

and

$$F_A = \frac{\pi}{2}(1.94)(1.09 \times 10^6)\frac{28.125}{(12)^4} = 4531 \text{ lbf.}$$

The minimum compressive yield strength of plexiglass is 12,000 psi.

Poisson's ratio of plexiglass is approximately 0.384.

The shape and dimensions of a section of the front face are

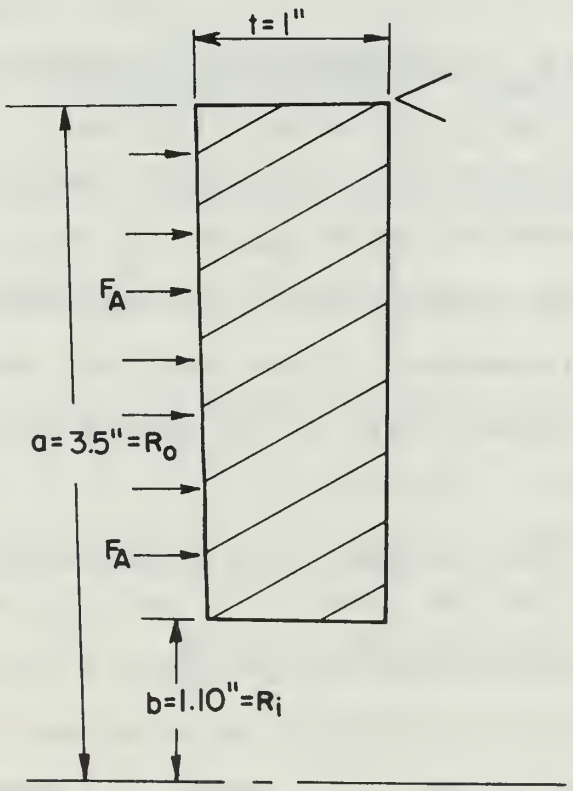

From Roark [Ref. 10] for a flat plate with a small concentric circular hole, uniformly loaded, outer edge simply supported; an expression for the maximum unit stress at the plate surface is

$$\sigma_{max} = \frac{3\ w\ a^2(3m+1)}{4mt^2}$$

where w = unit applied load = $\frac{F_A}{\pi(a^2-b^2)}\ \frac{lb}{IN^2}$

a = outer radius of plate (IN)

b = outer radius of center hole (IN)

t = thickness of plate (IN)

m = reciprocal of Poisson's ratio

$$w = \frac{4531}{\pi(3.5^2-1.1^2)} = 130.5\ \frac{lbs}{IN^2}$$

$$m = \frac{1}{.384} = 2.6$$

$$\sigma_{max} = \frac{(3)(130.5)(3.5)^2[3(2.6)+1]}{(4)(2.6)(1.00)(1.00)} = 4044\ \frac{lb}{IN^2}$$

An aluminum ring with slightly oversized holes for the bolts was used around the outside edge to help distribute the stresses. A more fixed edge support results. True edge fixity is very difficult to obtain in practice. A more complicated stress formula for a fixed edge is given in Ref. 10. The maximum stress using this formula is 1090 psi.

The yield strength of the plexiglass with a 25% factor of safety is

$$(0.75)(12,000) = 9000\ \frac{lb}{IN^2}$$

Therefore, a plastic face one inch thick is acceptable. Some batches of plexiglass exhibit yield strengths up to 16,000 psi. Also the front face was actually more than one inch thick due to the addition of a stator to the face.

C. BOLT STRESSES

Twelve ¼-28NF bolts were used to assemble the water brake (Figure 1). The stress area for one of these bolts is 0.0362 in^2 [Ref. 8] and the tensile strength of machinery steel bolts varies from 60,000 to 100,000 psi. One 60,000 psi bolt is capable of resisting

$$(60{,}000 \frac{lbs}{IN^2})(.0362\ IN^2) = 2172 \text{ lbs of force}$$

The twelve bolts can support

$$(2172)(12) = 26{,}064 \text{ lbs of force.}$$

This gives a large margin of safety.

Four 12-28NF flat head machine screws could be used to attach each stator to the face. The screws have a tensile strength of 100,000 psi and a stress area of 0.0256 IN^2. Each screw could thus support

$$(100{,}000 \frac{lb}{IN^2})(.0256\ IN^2) = 2560 \text{ lbs of force.}$$

Each screw is capable of supporting 80 IN-lb of shear stress [Ref. 9] which would give a total of 640 IN-lb for eight screws if all of them were acting to resist shear. However, it was found in practice that four 8-36NF screws were sufficient for attaching the stators because friction between the stator and face helps to resist rotation of the stator, and some of the absorbed torque is transmitted directly to the case by water passage through the shroud. Also, part of the force acts as a tensile stress on the screws.

REFERENCES

1. Van Zelm Associates, Inc., Report 279, Design Study for Rotary Energy Absorber, by C. Cometta, submitted to Naval Air Engineering Center under Contract No. N00156-68-C-2447, January 1969.

2. Commons, P. M., Instrumentation of the Transonic Turbine Test Rig to Determine the Performance of Turbine Inlet Guide Vanes through the Application of the Momentum and Moment of Momentum Equations, MSAE Thesis, Naval Postgraduate School, September 1967.

3. Lenzini, M. J., Calibration of Turbine Test Rig with Impulse Turbine at High Pressure Ratios, Aeronautical Engineer's Thesis, Naval Postgraduate School, June 1968.

4. Esdaile, S. G., An Investigation of a Transonic Turbine Test Rig, MSAE Thesis, Naval Postgraduate School, October 1969.

5. Schlichting, H., Boundary-Layer Theory, 6th ed., p. 606-610, McGraw-Hill, 1968.

6. Shepherd, D. G., Principles of Turbomachinery, Macmillan, 1956.

7. Shigley, J. E., Dynamic Analysis of Machines, McGraw-Hill, 1961.

8. Esbach, O. W., Handbook of Engineering Fundamentals, 2d ed., p. 1-202 to 1-203, Wiley, 1952.

9. American Society of Tool Engineers, Tool Engineers Handbook, p. 1173-1177, McGraw-Hill, 1949.

10. Roark, R. J., Formulas for Stress and Strain, 3rd ed., p. 192-198, McGraw-Hill, 1954.

INITIAL DISTRIBUTION LIST

		No. Copies
1.	Defense Documentation Center Cameron Station Alexandria, Virginia 22314	20
2.	Library, Code 0212 Naval Postgraduate School Monterey, California 93940	2
3.	Commander, Naval Air Systems Command Navy Department Washington, D. C. 20360	1
4.	Professor M. H. Vavra Department of Aeronautics Naval Postgraduate School Monterey, California 93940	3
5.	Chairman, Department of Aeronautics Naval Postgraduate School Monterey, California 93940	1
6.	Professor R. D. Zucker Department of Aeronautics Naval Postgraduate School Monterey, California 93940	1
7.	Dr. E. S. Lamar (Code 03C) Chief Scientist, Research and Technology Naval Air Systems Command Navy Department Washington, D. C. 20360	1
8.	Mr. W. J. Kaufman Naval Air Engineering Center Philadelphia, Pennsylvania 19112	1
9.	Dr. O. H. Johnson Naval Air Systems Command (Code 330B) Navy Department Washington, D. C. 20360	1
10.	Dr. H. J. Mueller Naval Air Systems Command (Code 310) Navy Department Washington, D. C. 20360	1

11. Mr. I. Silver, Code 330 — 1
Propulsion Administrator
Research and Technology
Naval Air Systems Command
Navy Department
Washington, D. C. 20360

12. Office of Naval Research — 1
Air Programs Office
Navy Department
Washington, D. C. 20360

13. Office of Naval Research (Power Branch) — 1
Attn: Mr. J. K. Patton, Jr.
Navy Department
Washington, D. C. 20360

14. Dr. F. I. Tanczos, Code 033 — 1
Technical Director, Research and Technology
Naval Air Systems Command
Navy Department
Washington, D. C. 20360

15. LT T. A. Mercer, USN — 1
Attack Squadron 122
Lemoore Naval Air Station
Lemoore, California 93245

Security Classification

DOCUMENT CONTROL DATA - R & D

(Security classification of title, body of abstract and indexing annotation must be entered when the overall report is classified)

1. ORIGINATING ACTIVITY (Corporate author)	2a. REPORT SECURITY CLASSIFICATION
Naval Postgraduate School Monterey, California 93940	Unclassified
	2b. GROUP

3. REPORT TITLE

The Development of a Water Dynamometer for Turbine Test Applications

4. DESCRIPTIVE NOTES (Type of report and inclusive dates)

Master's Thesis; October 1969

5. AUTHOR(S) (First name, middle initial, last name)

Thomas Alexander Mercer

6. REPORT DATE	7a. TOTAL NO. OF PAGES	7b. NO. OF REFS
October 1969	114	10

8a. CONTRACT OR GRANT NO.	9a. ORIGINATOR'S REPORT NUMBER(S)
b. PROJECT NO.	
c.	9b. OTHER REPORT NO(S) (Any other numbers that may be assigned this report)
d.	

10. DISTRIBUTION STATEMENT

This document has been approved for public release and sale;
its distribution is unlimited.

11. SUPPLEMENTARY NOTES	12. SPONSORING MILITARY ACTIVITY
	Naval Postgraduate School Monterey, California 93940

13. ABSTRACT

This study describes the design and development of a water dynamometer capable of absorbing and measuring a variable torque on a shaft rotating at velocities up to 20,000 revolutions per minute. The dynamometer was specifically designed to absorb a minimum of 117 horsepower at 10,000 RPM for use in the testing of small single stage turbines. The effects of various internal rotor and stator arrangements, water flow rates, internal clearances, and methods of torque variation and control were investigated. A method of extending the results of this study to the design of geometrically similar machines of larger size and increased torque absorption capacity was formulated.

DD FORM 1 NOV 65 1473 (PAGE 1)

S/N 0101-807-6811

Security Classification

A-31408

14. KEY WORDS	LINK A		LINK B		LINK C	
	ROLE	WT	ROLE	WT	ROLE	WT
Water Dynamometer						
Water Brake						
Turbine Tests						
Water Turbine						
Turbomachinery Design and Test						
Dimensional Analysis						